sustainability

MDPI

Review

Linear Permanent Magnet Vernier Generators for Wave Energy Applications: Analysis, Challenges, and Opportunities

Reza Jafari [1], Pedram Asef [2,3,*], Mohammad Ardebili [1] and Mohammad Mahdi Derakhshani [1]

[1] Electrical Engineering Department, K. N. Toosi University of Technology, Tehran 1631714191, Iran
[2] Department of Electronic and Electrical Engineering, University of Bath, Bath BA2 7AY, UK
[3] Department of Engineering and Technology, University of Hertfordshire, Hatfield AL10 9AB, UK
* Correspondence: p.asef@herts.ac.uk

Abstract: Harvesting energy from waves as a substantial resource of renewable energy has attracted much attention in recent years. Linear permanent magnet vernier generators (LPMVGs) have been widely adopted in wave energy applications to extract clean energy from oceans. Linear PM vernier machines perform based on the magnetic gearing effect, allowing them to offer high power/force density at low speeds. The outstanding feature of providing high power capability makes linear vernier generators more advantageous compared to linear PM synchronous counterparts used in wave energy conversion systems. Nevertheless, they inherently suffer from a poor power factor arising from their considerable leakage flux. Various structures and methods have been introduced to enhance their performance and improve their low power factor. In this work, a comparative study of different structures, distinguishable concepts, and operation principles of linear PM vernier machines is presented. Furthermore, recent advancements and innovative improvements have been investigated. They are categorized and evaluated to provide a comprehensive insight into the exploitation of linear vernier generators in wave energy extracting systems. Finally, some significant structures of linear PM vernier generators are modeled using two-dimensional finite element analysis (2D-FEA) to compare their electromagnetic characteristics and survey their performance.

Keywords: direct-drive; finite element analysis; high force density; linear permanent magnet vernier machine; linear generator; magnetic gearing effect; wave energy

Citation: Jafari, R.; Asef, P.; Ardebili, M.; Derakhshani, M.M. Linear Permanent Magnet Vernier Generators for Wave Energy Applications: Analysis, Challenges, and Opportunities. *Sustainability* **2022**, *14*, 10912. https://doi.org/10.3390/su141710912

Academic Editor: Gaetano Zizzo

Received: 25 July 2022
Accepted: 25 August 2022
Published: 1 September 2022

1. Introduction

Rotational electrical machines equipped with linear to rotary motion converters had been employed for linear applications before the introduction of linear structures [1]. Even though linear motion can be realized by using rotational machines and linear to rotary motion converters, some unfavorable concerns are inevitably arisen, including higher costs, lower accuracy of position sensing, higher inertia, higher maintenance, and shorter lifetime of the system [2]. Hence, devices to transform the linear to the rotary motion were eliminated and replaced by linear machines as more profitable alternatives. Linear structures have been broadly employed in different applications such as rail transit systems [3], ropeless elevators [4,5], automatic doors [6], electromagnetic suspension systems [7], free-piston engines [8,9], and wave energy applications [10]. The main scope of this research is to investigate the utilization of linear machines in harvesting wave energy, known as one of the most significant renewable energy resources.

The utilization of wave energy conversion systems has become extensively pervasive to generate electrical power [11,12]. Wave energy has the highest power density among other resources of renewable energy and is also more predictable. The capacity of ocean wave energy was estimated between 8000 to 80,000 TW·h/yr or 1 to 10 TW, indicating the importance of wave energy conversion technology [13]. However, this technology is moderately immature in comparison with other consequential energy resources, such

as wind [14] and solar energy [15,16]. In order to harvest the environmentally friendly wave energy of oceans, wave energy converters (WECs) are employed. The devices to harness wave energy are categorized based on different criteria, such as the wave direction or their operation principles [17]. Two of the most widely used WECs that can be integrated with linear generators are Archimedes wave swing (AWS) and point absorber converters. Linear generators can produce electricity from the reciprocating motion of waves yielded by wave energy converters [18]. Different types of linear generators have been proposed, such as linear permanent magnet synchronous generators (LPMSGs) [19], linear flux-switching permanent magnet generators [20], and linear permanent magnet vernier generators (LPMVGs) [21].

Linear PM synchronous generators are outstanding options for wave energy harvesting due to offering high power capability and high efficiency [22,23]. On the other hand, the study on magnet materials and the improvement of their characteristics, specifically neodymium–iron–boron (NdFeB) magnets, have led to growing attention on PM machines [24]. However, a high number of poles are required for linear PM synchronous generators to be able to provide a high power density [25,26]. Linear PM vernier generators are regarded as excellent candidates for this aim. Linear vernier structures operate based on the same principles as magnetic gears, known as the magnetic gearing effect, which enables them to offer a high power/force density at low speeds [27]. A linear magnetic gear with the capability of adjustable gear ratio was surveyed in [28] used in wave energy conversion systems. The integration of a linear tubular magnetic gear and a tubular PM generator was proposed in [29] for extracting wave energy with a higher power density at low speeds. Even though magnetic gears deliver a high power density, the integration of magnetic gears and linear generators makes the system suffer from a bulky size and a complicated structure. Accordingly, linear PM vernier machines (LPMVMs) are preferable, in which they function based on the principles of magnetic gearing effect [30]. Different configurations and novel structures of linear PM vernier machines have been proposed in numerous pieces of research. Despite the merit of the high power capability of linear PM vernier structures, they inherently possess a low power factor. The poor power factor of vernier structures has resulted from their high leakage flux, stemming from the magnetic gearing effect. Consequently, high rating converters should be employed for low power factor structures, which is not an economically viable solution [31]. In recent years, different methods have been suggested to enhance the poor power factor of linear vernier machines. Furthermore, the longitudinal end effect of linear vernier machines is regarded as the other problem which uniquely exists for linear structures compared to rotational ones. Linear machines have two open ends contrary to the rotational structures, leading to the undesirable longitudinal end effect and causing a high force ripple [32].

In recent years, different types of linear PM vernier generators have been proposed to further enrich their high power/force capability and diminish their unwanted disadvantages. A comprehensive study is required to offer a comparative analysis and study of different linear vernier generators for more investigation in the future. This research focuses on surveys that have been accomplished to improve the performance of linear PM vernier machines, specifically for wave energy applications. In addition, different concepts of linear vernier generators are evaluated, and operation principles are investigated in this paper. In Section 2, the significance of wave energy harvesting and a succinct description of wave energy systems will be explained. The operation principles and analysis of the linear PM vernier machines will be surveyed in Section 3. Different types of LPMVMs will be categorized and studied in Section 4. The solutions to improve the performance of linear vernier structures will be investigated in Section 5 based on a generic classification. Moreover, four outstanding structures of linear generators will be thoroughly examined and compared in Section 6 by employing two-dimensional finite element analysis (2D-FEA). Finally, the conclusions and some suggestions for future research on this topic will be drawn in Section 7.

2. Wave Energy Applications

The motivation to handle the environmental issues and also the necessity to eradicate the dependence upon fossil fuels have encouraged many researchers to seek clean and free renewable resources of energy [33–35]. Among the significant renewable energy resources, including wind and solar energy, wave energy offers the highest power density. Approximately 15 to 20 times more energy per square meter can be harnessed by using wave energy of oceans in comparison with wind energy [36]. In addition, wave energy is more predictable and leaves fewer adverse impacts on the environment. Wave energy extraction systems can generate electricity for approximately 90% of the time, while the availability of other vital resources of renewable energy is 20% to 30% [37]. The distribution of mean power per year that can be harvested from waves is shown in Figure 1.

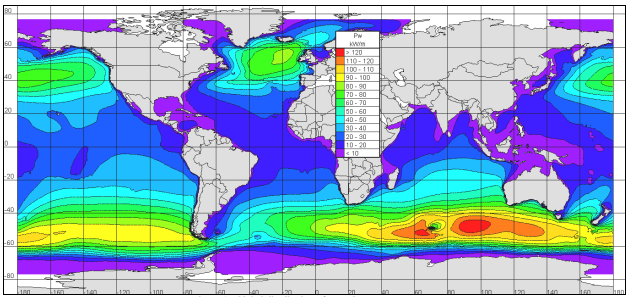

Figure 1. Distribution of mean power per year harvested from ocean waves [38].

It can be inferred that there are outstanding opportunities to exploit the energy from oceans; principally, the southern hemisphere is more prosperous in terms of wave energy extracting capabilities. Moreover, the installation of wave energy systems is predicted to reach 100 *GW* in Europe by 2050, which can supply the electricity required by 76 million households [39]. This shows the tremendous possibilities for many countries to benefit from a clean and free resource of energy. However, there are some regions in the world that are deprived of this kind of energy due to their inaccessibility to oceans.

Research on the prospects of extracting wave energy and the introduction of practical devices to transform the motion of waves into electrical power is increasingly required. Many researchers work on developing novel structures and improving the technology of wave energy conversion from oceans [40–42].

2.1. Wave Energy Converters (WECs)

In order to extract the energy from waves, wave energy converters are extensively employed, which can be classified into several categories based on different criteria. In this paper, wave energy conversion systems are classified based on their principles of operation [43–45], as follows:

- oscillating water column;
- overtopping converter;
- oscillating body system.

Among the mentioned classifications, four types of oscillating body converters perform based on linear power take-off systems. Oscillating water column and overtopping converters use rotational generators to produce electricity [46]. The study of wave energy converters is beyond the scope of this research. Therefore, two of the most commonly used WECs that can be integrated with linear generators are surveyed, i.e., Archimedes wave swing (AWS) and point absorber converters.

2.1.1. Archimedes Wave Swing WEC

Generally, Archimedes wave swing systems are compromised of a chamber filled with air and a floater attached to the translator of a linear generator. AWS converters function based on the difference in the air pressure of the chamber. The movement of waves provides

the translator of a linear generator with reciprocal motion. As the waves pass over the AWS, the floater heaves downward, and the air inside the chamber is compressed. In addition, when the AWS is placed under a trough wave, the air pressure causes the floater to move upward in parallel to the movement of the linear generator. The concept of harvesting wave energy by using AWS converters is depicted in Figure 2.

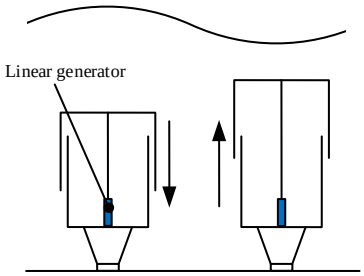

Figure 2. Concept of harvesting wave energy based on AWS converters.

The AWS is an off-shore converter and is entirely submerged. Hence, AWS converters possess the advantages of being protected from storms, not imposing obstacles for ships, and being rescued from human disturbance. However, the maintenance is complicated, and the installation is demanding [47].

2.1.2. Point Absorber WEC

Linear generators can be driven to produce electricity through the utilization of point absorber converters. Point absorber devices can harvest wave energy from all directions and convert the wave movements into electricity using a linear generator. The simplicity of prototyping and installing point absorber devices has made them promising candidates for wave energy applications [48,49]. Nevertheless, the weak performance of point absorbers in conditions that the frequency of the wave and the frequency of the converter differ leads to the requirement for more advanced controlling mechanisms. Otherwise, the efficiency of the system decreases considerably [50]. The necessity to tune the wave energy converter to be in resonance with the frequency of waves has led to the introduction of two-body point absorbers, in which the active control is not required anymore [51]. Two-body point absorbers extract wave energy from the relative motion between the buoy and the submerged body [52]. The straightforward configurations of single-body and two-body point absorber converters are illustrated in Figure 3. As can be seen, a two-body converter is compromised of a surface body and a submerged body, which are connected to the linear generator. The surface body performs as an energy harvester, and the submerged body creates inertia to assist the converter in having a more resonant frequency with waves.

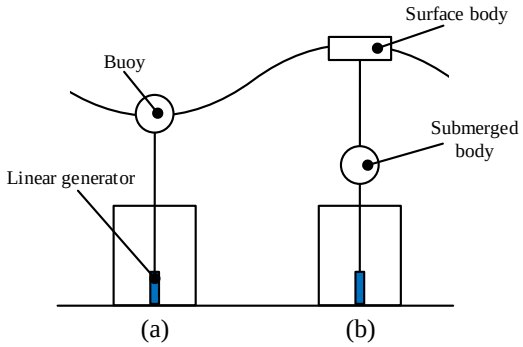

Figure 3. Concept of harvesting wave energy based on point absorber converters: (**a**) single-body, and (**b**) two-body point absorber converters.

2.2. Linear Generators

A power take-off (PTO) system is employed in capturing wave energy to transform the mechanical motion into electricity. A PTO system contains a linear generator or a rotational electrical generator connected to a mechanical interface, such as air turbines, hydraulic, hydro turbines, or mechanical direct-drive systems. Air turbines are used to convert the wave energy into the mechanical energy required by the rotational generator, which is primarily employed in oscillating water column systems and operates based on the concept of the oscillating water level. The hydraulic converters perform as mechanical interfaces to drive the rotational generators in wave energy conversion systems through the activation of the hydraulic arm or piston and the pressure increase of the hydraulic oil. Overtopping devices or hydraulic pump systems use hydro turbines to be used in wave energy extraction systems. The mechanical direct-drive systems are the other types of mechanical interfaces to connect the wave energy converter to the electrical generator. The utilization of rotational electrical generators connected to the mechanical interfaces can lead to higher maintenance, lower reliability, and decreased efficiency [53,54].

An efficient strategy to extract wave energy from oceans is adopting direct-drive linear generators, in which the oscillatory motion of waves can be converted into electrical power without any intermediate equipment. The importance of linear structures in extracting wave energy cannot be denied owing to being less complicated, less bulky, and more efficient compared to conventional rotational generators [55,56]. Various kinds of linear generators have been commercialized and widely used in wave energy conversion systems. Correspondingly, a point absorber wave energy converter based on the direct-drive linear PM generator was developed at Uppsala University [57] to provide a less complicated system. In addition, a wave energy harvesting device integrated with a linear PM generator was proposed at Oregon State University [58].

Despite the outstanding merits of linear generators used in wave energy harvesting, they have some weaknesses. The frequency and amplitude of the voltage supplied by the linear generator are not constant during their operation, which complicates the transmission of power [59]. Although linear PM generators offer high power density, they are costly, and PMs are at the risk of demagnetization. In addition, conventional PM synchronous generators possess a bulky size and need a high number of poles to offer a high power density at low speeds. Consequently, linear PM vernier generators can be practical solutions with improved performance; the rest of this research focuses on linear vernier structures.

3. Operation Principles and Analysis of Linear PM Vernier Machines

The concept of linear vernier structures is developed based on rotational machines, as shown in Figure 4.

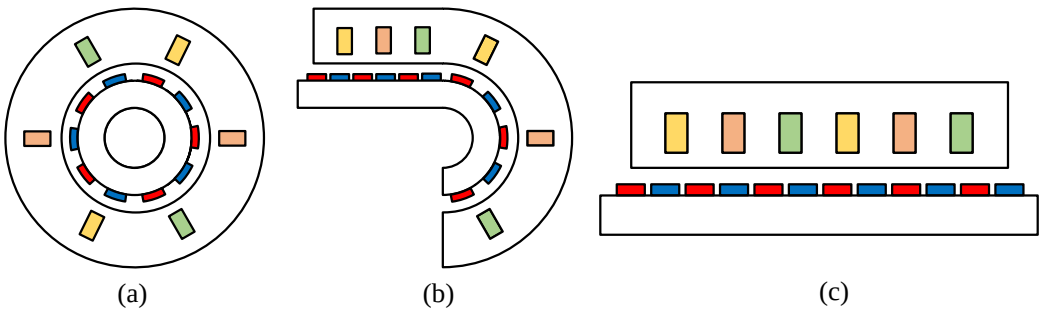

Figure 4. Development of a linear structure based on the rotational concept: (**a**) Rotational machine, (**b**) Unrolling a rotational machine into a linear machine, and (**c**) A linear machine.

Accordingly, the linear to motion converters can be eliminated, and the linear movement can be generated by using a linear structure and without additional equipment. Linear PM vernier machines can produce a high power/force density at low speeds, an outstanding feature, particularly for wave energy applications. Linear PM vernier machines

function based on the magnetic gearing effect, which makes them distinguishable from linear PM synchronous counterparts. Accordingly, the operation principles of linear vernier structures must be surveyed initially.

3.1. Magnetic Gearing Effect

Mechanical gearbox systems have been used to connect the moving part of electrical machines to the load to transfer speed and torque/force. In recent years, magnetic gears have become more prevailing in several applications [60]. Therefore, mechanical gearbox systems can be superseded by magnetic gears, and the following advantages can be accomplished effectively [61–63]:

- no need for maintenance;
- isolation between the output and input shafts;
- inherent overload protection;
- no mechanical vibration and minimum acoustic noise;
- higher efficiency;
- higher reliability;
- no need for lubrication.

A rotational magnetic gear system was firstly introduced in [64], providing high torque capability. Until recently, different structures have been developed from magnetic gears and are used in different applications, including wave energy conversion [65]. A radial flux magnetically geared generator was proposed in [66], designed for wave energy applications. The proposed structure is depicted in Figure 5 and offers a high power capability. Nevertheless, the proposed structure utilizes a huge amount of magnets and has a complicated structure.

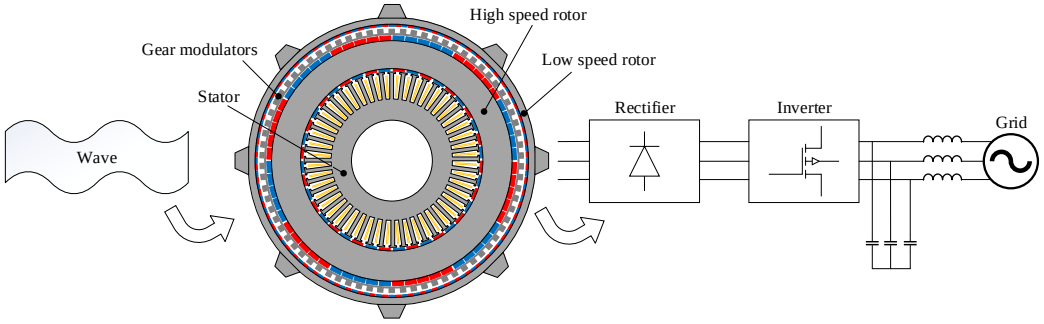

Figure 5. A radial flux magnetically geared generator used in wave energy harvesting.

Owing to the notable benefits acquired by magnetic gear systems, diverse types of linear magnetic gears have been conceptualized and introduced. For the first time, a linear magnetic gear was proposed by K. Atallah et al. [67], based on the magnetic gearing effect. The proposed linear magnetic gear adopts the tubular structure, offering high thrust force capability. Similar to rotational magnetic gears, a conventional linear magnetic gear consists of a low-speed mover with a higher number of poles, a high-speed mover with a fewer number of poles, and a stationary part (ferromagnetic pole pieces). The ferromagnetic pole pieces modulate the magnetic field of the mover with a different number of poles. Thus, in order to take advantage of the magnetic gearing effect, the number of ferromagnetic pole pieces of the stationary part must be equal to the sum of the number of pole pairs of the moving parts.

A linear magnetic gear system comprises a linear magnetic gear and a conventional linear PM synchronous machine (LPMSM), in which the inner translator of the linear magnetic gear is connected to the translator of the PM machine. The inner translator of the linear magnetic gear can be replaced by the stator of the LPMSM if they have the same number of poles. In the next step, the stator and ferromagnetic pole pieces of the system can be integrated as stationary parts in order to result in the concept of linear vernier

structures. Linear vernier machines are introduced based on the concept of the magnetic gearing effect. However, less permanent magnet volume is adopted compared to magnetic gear systems, and vernier structures possess smaller dimensions because of the integration of ferromagnetic pole pieces with the stator teeth. Accordingly, linear PM vernier machines are perceived as excellent options for harvesting wave energy. The stator teeth of a linear vernier machine perform as the modulators and conduct the modulation of the airgap magnetic field of the translator to adapt to the stator magnetic field with different poles. In order to exploit the magnetic gearing effect, the following relationship of slot/pole combination must be satisfied:

$$Z_r = Z_s \pm p \tag{1}$$

where Z_r is the number of translator pole pairs, p is the number of stator armature winding pole pairs, and Z_s is the number of stator teeth. The electrical speed of the mover of a linear vernier machine equals the effective flux electrical speed; consequently, the following equation can be used to define the mechanical speeds.

$$v_{eff} = GR \times v \tag{2}$$

The effective flux pitch is also expressed as:

$$\tau_{eff} = \frac{1}{2} GR \times \tau_m \tag{3}$$

where v_{eff} is the mechanical speed of the effective flux, v is the mechanical speed of the moving part, τ_{eff} is the pitch of the effective flux, and τ is the tooth pitch of the mover. Based on the relationships, the mechanical speed of the effective flux is greater than the translator speed, which is resulted from the magnetic gearing effect of vernier machines.

Contrary to conventional PM synchronous machines, linear vernier structures possess two airgap components, i.e., the fundamental component (Z_rth order) and the modulated component ($Z_s \pm Z_r$th order). The back-EMF is produced as a result of the interaction between the fundamental component of magnetomotive force (MMF) produced by PMs (Z_rth order) and the airgap permeance of stator slots (Z_sth order). The reciprocal velocity of the modulated component of $|Z_s - Z_r|$th order is $Z_r/(Z_s - Z_r)$ times greater than the fundamental component. This ratio is known as the gear ratio of vernier machines. The higher the gear ratio, the higher velocity of the modulated component is expected; accordingly, a higher back-EMF can be obtained [68]. Indeed, linear PM vernier machines undergo a significant flux change in a short displacement of the translator owing to the utilization of the magnetic gearing effect, providing a higher thrust force density.

3.2. Analysis and Optimization of Linear PM Vernier Generators

The fundamental relationships and operation principles of linear PM vernier machines are required to be studied to analyze their characteristics. Different methods to investigate vernier structures had been carried out, which failed to explain their characteristics accurately. The design principles of vernier structures were investigated carefully by Kim et al. [69], and a reliable analysis was accomplished for the first time. The analytical analysis of a linear vernier machine was realized in [70] based on flux harmonic theory. In addition, two structures of surface-mounted and consequent-pole LPMVMs were analytically surveyed in [71]. Although the proposed procedure can be accomplished in a short time, the analysis did not consider the magnetic saturation and longitudinal end effect. A nonlinear equivalent magnetic network (EMN) was developed in [72] to survey the performance of a linear PM vernier machine by considering the cogging force and end effect. A novel mesh generation approach was studied in [73] based on equivalent magnetic network modeling to increase the accuracy. Linear vernier structures can be optimized to offer more beneficial performance in different applications. A multi-objective optimization method was carried out in [74] in order to improve the performance of a linear PM vernier machine. In addition, a linear vernier structure with the capability of high fault

tolerance was proposed in [75] and optimized to meet the requirement of a multi-objective optimization process.

High leakage flux of linear PM vernier structures is a considerable problem that can deteriorate their ideal operation. Generally, the kinds of leakage flux in a linear PM vernier machine can be divided into tooth-tip leakage flux, air-gap leakage flux, and magnet-end leakage flux for a surface-mounted LPMVM. An analytical procedure was carried out in [76] to survey the tooth-tip leakage flux of the linear vernier structure based on the translator position. In addition, the fringing flux was considered into account. However, many approximations were regarded, decreasing the accuracy of the analysis, such as neglecting the saturation effect and ignoring the longitudinal end effect. Reducing the leakage flux of vernier machines is aimed by many researchers to improve the performance of vernier structures, which will be thoroughly discussed in this paper.

4. Linear Permanent Magnet Vernier Generators (LPMVGs)

Linear PM vernier generators are extensively employed in wave energy systems. In order to provide a comprehensive study and investigate the performance of linear PM vernier structures, they can be classified into the following major categories, as shown in Figure 6:

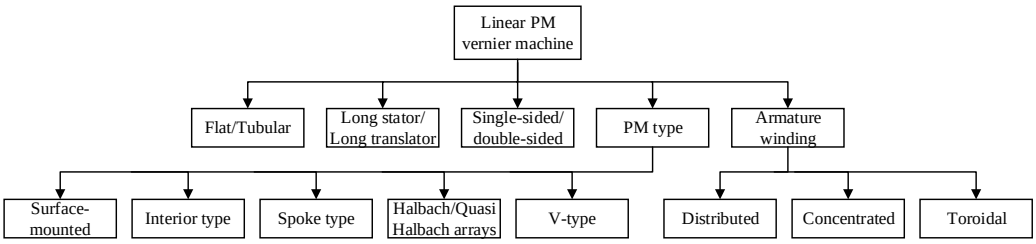

Figure 6. General classification of LPMVMs based on design characteristics.

- linear flat and tubular;
- long/short stator and short/long translator;
- single-sided and double-sided;
- permanent magnet type;
- armature winding.

4.1. Flat and Tubular Structures

Linear PM vernier machines can be divided into two primary classifications of flat and tubular structures, which have been commercialized and used in wave energy applications. Some unconventional types of linear generators have also been proposed but are not efficient choices, such as octagonal linear PM generators [77] or four-sided linear generators [78]. In both linear flat and tubular structures, the stator is the stationary part, and the translator is driven by a wave energy converter to extract the reciprocal motion of waves [79,80].

A hybrid tubular PM vernier generator used in wave energy applications was proposed in [81], in which the armature windings and magnets are located on the stator. The hybrid tubular machine was developed from a linear PM vernier configuration depicted in Figure 7, offering higher flux density compared to the linear flat counterpart. The process of developing the tubular vernier generator from the flat structure is illustrated in Figure 8. Due to the higher ratio of force to weight for the tubular structure, the active volume can be decreased.

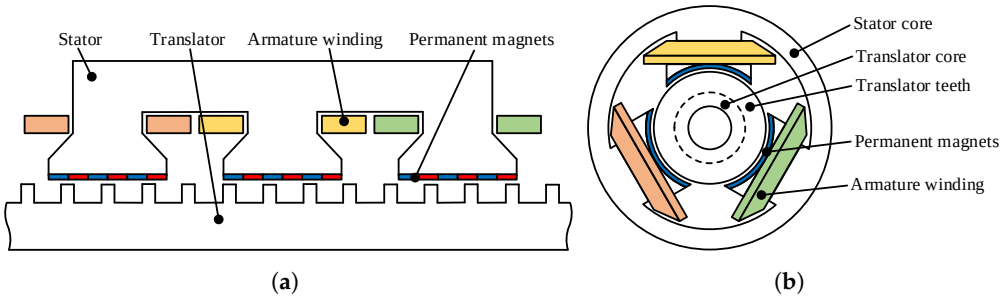

Figure 7. A hybrid tubular PM vernier generator, (**a**) flat structure, and (**b**) tubular structure.

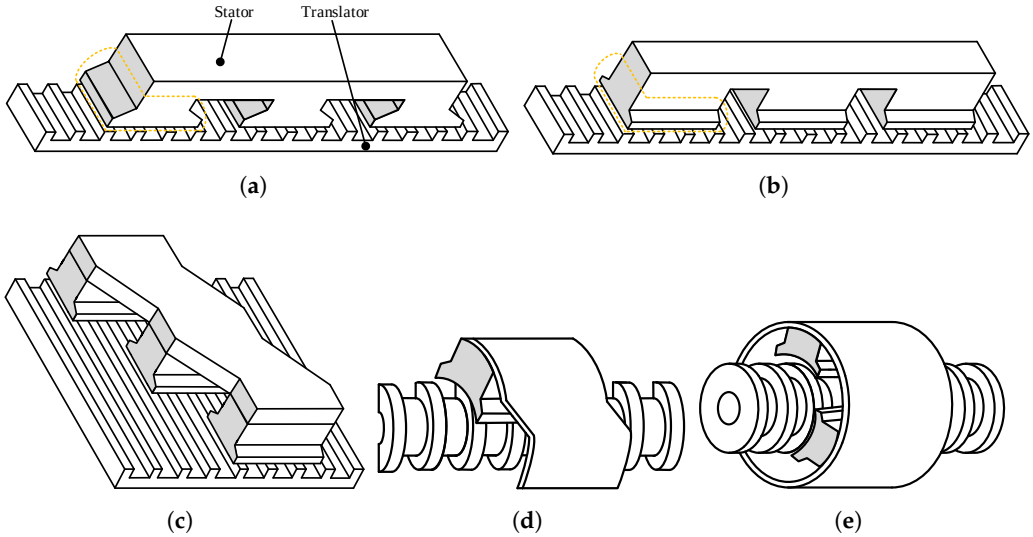

Figure 8. The process of developing the flat to the hybrid tubular PM vernier generator: (**a**) flat structure, (**b**) developing the flat to tubular step one, (**c**) developing the flat to tubular step two, (**d**) developing the flat to tubular step three, and (**e**) the tubular structure.

A high temperature superconducting dual stator tubular vernier machine (HTS-DSTVM) was proposed in [82], using HTS bulks to improve flux linkage. A two-dimensional cross-section of the tubular linear PM vernier generator is shown in Figure 9. The armature windings are only located on the outer stator, and HTS bulks are inserted inside the teeth of the inner stator. Although the HTS tubular generator offers a high thrust force density, the structure is relatively costly and complicated.

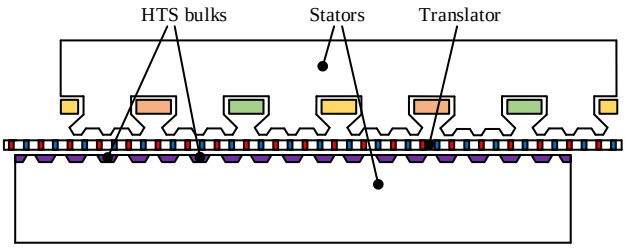

Figure 9. A high temperature superconducting dual stator tubular vernier machine (HTS-DSTVM).

Tubular and flat vernier machines perform based on the same operation principles but have different topologies. Tubular structures are symmetrical around an axis; therefore, the forces are applied from all directions. In addition, their symmetrical structure provides a more uniform distribution of magnetic flux compared to flat counterparts [83–85]. However, the complexity of prototyping and analysis of tubular structures is the most

deterrent element that has pushed researchers to pay more attention to linear flat machines. Correspondingly, this paper concentrates more on linear flat vernier configurations.

4.2. Long/Short Stator and Short/Long Translator

Another criterion to compartmentalize linear PM vernier machines is based on the structures of the stator and translator, i.e., long stator and short translator or short stator and long translator. The moving part of a linear vernier machine with a short stator and long translator is longer than the stator, in which the preponderance of linear PM vernier machines belongs to this sort. A part of the long stator of a linear vernier machine with a short moving part is not interacting with the translator. Hence, the copper losses increase if the armature windings are located on the stator. An approach is disconnecting the redundant part of the stator with the aid of power electronic converters. However, the system becomes complex, and the costs grow due to the employment of additional equipment. An alternative strategy to avoid these problems and reduce the costs is locating both armature windings and magnets on the short moving part and adopting a reluctance core for the long stationary part [86]. However, using a moving translator equipped with armature windings is also a challenging concern for designers.

4.3. Single-Sided and Double-Sided

Single-sided linear structures have been developed from the rotational concept of electrical machines, possessing only a stator and a moving part [87]. An attraction force exists in the vertical direction of the reciprocation of linear single-sided machines. This force is known as the normal force, which leads to a high thrust force ripple. In order to attenuate the normal force, double-sided structures are excellent choices. In addition, a higher power capability can be obtained by using a double-sided generator instead of the single-sided one [88].

4.4. Permanent Magnet Type

Different types of magnets can be adopted for linear PM vernier generators. As shown in Figure 10, magnet types can be classified into five major categories, and the other configurations are considered as subdivisions:

- surface-mounted type;
- interior type;
- spoke type;
- halbach/Quasi-Halbach arrays;
- V-type.

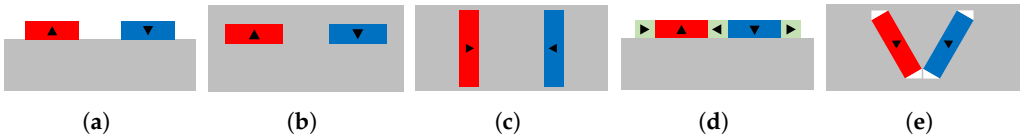

Figure 10. Different types of magnets: (**a**) Surface-mounted type, (**b**) Interior type (**c**) Spoke type, (**d**) Quasi-Halbach arrays, and (**e**) V-type.

Permanent magnets can be located on the surface of the stator or translator of linear vernier machines, known as the surface-mounted type. The surface-mounted magnets with a simple structure have been widely adopted for different linear vernier machines [89]. Surface-mounted PMs with the sinusoidal shape can be helpful in decreasing the back-EMF distortion [90]. Nevertheless, this type of magnet has not been used in many prototyped structures due to the highly increased cost of using magnets with a unique configuration. Permanent magnets are regarded as one of the most vulnerable and expensive parts of a linear PM vernier machine. The consequent-pole magnet type is considered a practical option to downsize the costs by decreasing the amount of PMs. By exploiting the consequent pole instead of surface-mounted PMs, not only the volume of PMs is considerably

reduced, but the leakage flux is also diminished. Figure 11 shows how the leakage flux in conventional surface-mounted and consequent-pole structures are produced.

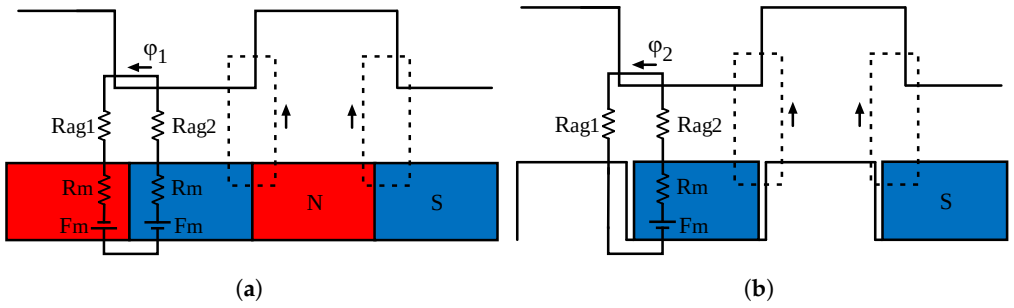

Figure 11. Leakage flux of (**a**) A conventional surface-mounted structure, and (**b**) A consequent-pole structure.

As can be seen, due to the elimination of PM poles that do not participate in the production of the flux linkage, the leakage flux of the consequent-pole type can be reduced [91]. The leakage flux of the surface-mounted structure (ϕ_1) and the consequent-pole structure (ϕ_2) can be calculated as follows:

$$\phi_1 = \frac{F_m}{R_m + \frac{R_{ag1}+R_{ag2}}{2}} \tag{4}$$

$$\phi_2 = \frac{F_m}{R_m + R_{ag1} + R_{ag2}} \tag{5}$$

where R_m is the reluctance of the magnet, R_{ag1} and R_{ag2} are the air-gap reluctance of the slot and tooth, respectively. By comparing the leakage flux of both structures, the following relationship can be concluded, indicating a lower leakage flux for the consequent-pole type:

$$\phi_1 > \phi_2 \tag{6}$$

Moreover, the leakage flux of a consequent-pole type can be further weakened by using the tapered ferromagnetic poles [92]. By optimizing the ratio of the ferromagnetic pole tip to the pole pitch, as shown in Figure 12, the machine performance can be improved.

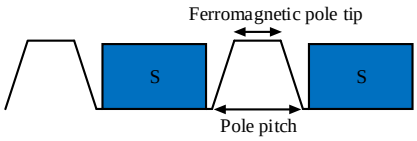

Figure 12. Tapered ferromagnetic consequent-poles.

A linear consequent pole stator permanent magnet vernier machine (LCPSPMVM) with improved force capability was compared with a surface-mounted counterpart in [93]. A 2D schematic of the consequent-pole linear machine can be seen in Figure 13.

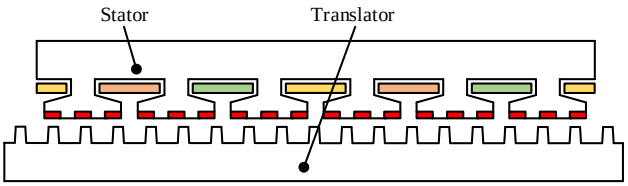

Figure 13. A linear consequent pole stator permanent magnet vernier machine (LCPSPMVM).

The volume of magnets for the consequent-pole machine is decreased by 25% compared to the surface-mounted counterpart with the same dimensions and design char-

acteristics. Despite using less PM volume, thrust force density is increased due to the reduction of the leakage flux. Nevertheless, due to the fact that the consequent-pole and surface-mounted structures have the same reluctance, a low power factor is expected for both types.

Interior magnet types are preferred over surface-mounted magnets to decrease the air gap length. There are different types of interior magnets [94–96]. Figure 10b shows a simple configuration of interior magnets with a linear shape. The usage of conventional interior magnets with a linear shape is restricted. In order to improve the flux linkage of linear vernier machines, other configurations are preferred, such as Halbach arrays or V-type magnets.

Spoke-type magnets have been exploited in different structures of linear vernier machines. Particularly, by adopting spoke-type magnets and the double-sided structure with a shift as half of the slot pitch, the flux focusing effect can be obtained. Thus, a higher power capability and power factor are anticipated [97].

In order to increase the flux linkage of linear PM vernier machines, Halbach arrays are excellent choices. A higher force density, self-shielding effect, low cogging force, and more sinusoidal distribution of airgap flux density are the advantages of Halbach magnets [98,99]. However, the construction process of Halbach magnets is complex, and the costs are increased. Accordingly, quasi-Halbach arrays are more profitable candidates. The configuration of quasi-Halbach magnets is shown in Figure 10d.

The V-type magnets can be regarded as a subclassification of interior types. However, V-type is an excellent solution to fulfill the flux focusing effect, which is preferred over the interior magnets with a linear shape. By employing V-type PMs for linear vernier machines, higher airgap flux density can be achieved, and the risk of irreversible demagnetization can be reduced [100]. Accordingly, higher thrust force density and higher power factor can be realized. The angle between two magnets and the dimensions can be optimized to improve the performance of V-type linear vernier structures. Furthermore, the iron bridges of the V-type magnets can be eliminated in order to decrease the leakage flux [101]. The bridged and bridgeless structures are compared in Figure 14.

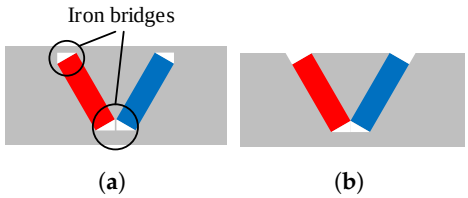

Figure 14. Different types of V-type permanent magnets: (**a**) bridged structure, and (**b**) bridgeless structure.

4.5. Armature Winding

Different types of distributed, concentrated, and toroidal windings can be used for the armature winding of a linear PM vernier machine. The distributed winding offers a more sinusoidal and higher back-EMF. On the other hand, by utilizing armature windings with fractional poles, more variety of slot/pole combinations can be adopted for linear machines contrary to rotational structures. Indeed, 0 and 360 mechanical degree positions do not coincide for a linear configuration, in which this feature uniquely provides linear vernier machines with the possibility to select a non-integer number of poles. A fractional pole-pair linear PM vernier machine (FP-LPMVM) with 18 slots and 3.5 armature pole pairs was proposed in [102]. The topology of the FP-LPMVM and the configuration of the armature winding are demonstrated in Figures 15 and 16, respectively. The proposed linear vernier machine offered a low thrust force ripple of 1.6%, owing to the unique configuration of winding and the combination of slots and poles.

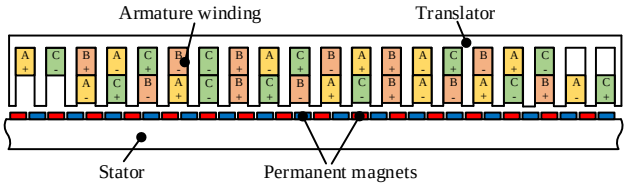

Figure 15. A fractional pole-pair linear PM vernier machine (FP-LPMVM).

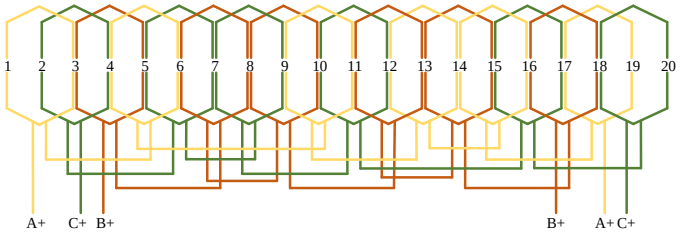

Figure 16. The winding layout of the FP-LPMVM.

However, the long end-windings cause the linear structure to suffer higher copper losses. Accordingly, concentrated winding for the armature of linear vernier machines is preferred in some cases due to a shorter end-winding and a higher capability of fault tolerance. In addition, the flux modulation poles (FMPs) have been utilized for the stator of a linear machine with concentrated windings in many cases. The modulation by FMPs instead of traditional teeth causes the fundamental flux components to have less interaction with the armature coils, leading to a lower force capability. Moreover, the toroidal winding type can be utilized for the armature winding of a linear PM vernier machine to decrease the length of end windings [103,104]. Not only the copper losses are decreased, but a higher fault-tolerant capability can also be obtained. However, the utilization of toroidal winding is restricted to some specific configurations of linear vernier structures.

5. Performance Improvement of Linear PM Vernier Generators

In order to increase the productivity of linear PM vernier machines in wave energy applications, their performance is required to be improved. As aforementioned, the most outstanding characteristic of vernier machines is their ability to offer high force/power at low speeds. Different configurations have been proposed to further develop the force density of linear PM vernier machines. On the other hand, many studies have concentrated on decreasing the negative sides of a linear PM vernier machine, including the reduction of leakage flux and the decrease of thrust force ripple. In addition, the cost and reliability of linear vernier generators are other concerns that must be taken into account. Overall, the methods to develop the operation of linear vernier generators are classified as:

- thrust force capability improvement;
- power factor development;
- thrust force ripple reduction;
- cost reduction.

5.1. Thrust Force Capability Improvement

The superiority of linear PM vernier machines is providing high thrust force density at low speeds, which is accounted outstanding merit and makes them different from linear PM synchronous machines. The capability of high thrust force of linear PM vernier structures originates from the principles of the magnetic gearing effect, which can be estimated by the following relationship [105]:

$$F = \frac{P}{v} = \frac{\sqrt{2}}{2} \frac{k_w B_{gmax} k_s L L_{stk}}{k_d} GR \quad (7)$$

where P is the electromagnetic power of the linear PM vernier machine, and v is the speed. k_w is the winding factor, B_{gmax} is the maximum flux density, k_s is the electric loading, k_d is the flux leakage coefficient, L is the effective length, L_{stk} is the stack length, and GR is the gear ratio. Equation (7) defines the parameters that directly influence the thrust force of a linear vernier structure. The gear ratio is a decisive parameter in which a higher force density can be obtained by selecting a high value of the gear ratio. In addition, by exploiting different configurations to increase the flux linkage, the force capability of vernier structures can be enhanced effectively [106,107].

A single-sided linear PM vernier machine with increased thrust force performance was proposed in [108], employing consequent-pole and Halbach PMs (CPHPMs). A 2D schematic of the CPHPM linear vernier machine is depicted in Figure 17a. As can be seen, Halbach arrays and armature winding are inserted inside the translator slots, and the stator employs the consequent-pole structure. Halbach arrays are the excitation source, and the stator teeth perform as the modulation pole-pieces. In addition, two other structures similar to CPHPM linear machine were studied, i.e., conventional surface-mounted and consequent-pole LPMVMs, as shown in Figure 17b,c. The proposed CPHPM LPMVM offers an average thrust force of 1.65 kN, while the surface-mounted and consequent-pole LPMVMs have an average force of 1.13 kN and 1.24 kN, respectively. By employing the proposed CPHPM linear vernier machine, thrust force density is improved by 46% and 33% compared to the surface-mounted and consequent-pole linear machines, respectively. However, the power factor of the proposed linear machine is decreased compared to the consequent-pole structure due to higher leakage flux. On the other hand, there are some considerations related to the reliability and the risk of demagnetization of the PMs of the CPHPM linear machine.

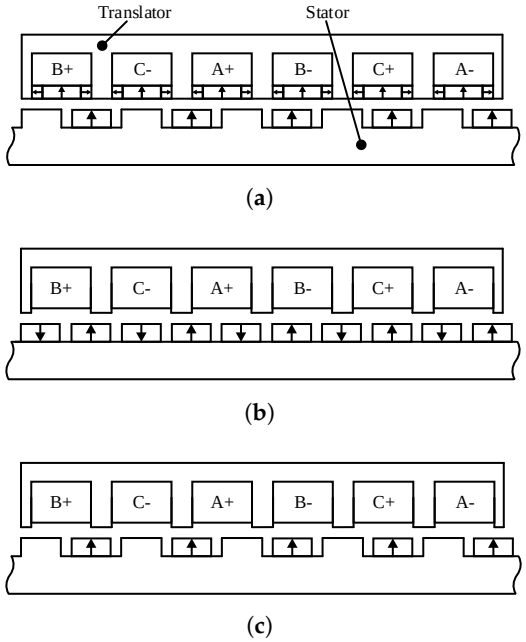

Figure 17. Linear PM vernier machines with increased thrust force capability, (**a**) LPMVM with consequent-pole and Halbach PMs (CPHPMs), (**b**) surface-mounted LPMVM, and (**c**) consequent-pole LPMVM.

5.2. Power Factor Development

The most critical drawback of linear PM vernier machines is their low power factor, which necessitates more consideration for vernier structures. Generally, the power factor of an electrical machine is defined as the ratio of the real power to the reactive power. Owing to the inherent low power factor of linear vernier structures, they require high rating converters to deliver the same real power. Indeed, the low power factor of vernier

machines becomes vital when the system is considered from the economic point of view. In recent years, many researchers have proposed different methods and configurations to enhance the performance of LPMVMs by developing their power factor. The power factor of vernier machines can be defined based on a phasor diagram, depicted in Figure 18.

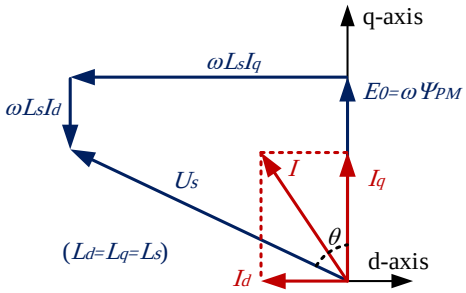

Figure 18. Phasor diagram of a PM vernier structure.

The power factor can be calculated by using the following realtionship [109,110], in which the resistance of the stator is neglected and the d-axis current equals zero:

$$cos\theta = \frac{1}{\sqrt{1 + \frac{L_s I}{\Psi_{PM}}}} \tag{8}$$

where L_s is the synchronous inductance, I is the current, and Ψ_{PM} is the flux linkage produced by PMs. Based on the classical method of calculating the power factor, increasing the flux linkage and decreasing the synchronous inductance leads to a higher power factor. The majority of research in this field can be divided into adopting the following approaches:

- optimal magnetic gear ratio;
- appropriate configuration of PMs;
- high-temperature superconducting (HTS) bulks.

5.2.1. Optimal Magnetic Gear Ratio

A principal step in defining the electromagnetic characteristics of linear PM vernier machines is selecting an optimal combination of slots and poles [111]. Different slot/pole combinations can be adopted for vernier structures based on the following expression [112]:

$$\frac{p \pm Z_r}{GCD(p \pm Z_r, p)} = mk \tag{9}$$

where m is the number of phases, k is an integer, and GCD is the greatest common divisor. For a linear PM vernier machine with PMs on the translator, the gear ratio is defined as the ratio of the number of translator PM pole pairs to the number of stator pole pairs.

$$GR = \frac{Z_r}{p} \tag{10}$$

Overall, higher values of gear ratio can lead to a higher force capability; nevertheless, due to the increment of the leakage flux, particularly the leakage flux resulting from PM fringing, the power factor decreases [113]. So, a practical way to improve the power factor is selecting a low gear ratio, while a considerable reduction of thrust force capability must be avoided. Certainly, a trade-off is required to be taken into account to offer a linear PM vernier machine with improved performance. In addition, a specific gear ratio can be obtained with different combinations when the ratio of the number of translator PM pole pairs and the number of stator pole pairs are constant.

5.2.2. Appropriate Configuration of PMs

An excellent approach to improving the power factor of linear vernier machines is adopting the appropriate configuration of magnets. Different types of magnets have been used in various structures to increase the flux linkage.

A dual-stator spoke-type linear vernier machine (DSSLVM) was proposed in [114]. In order to obtain the flux focusing effect, the stators are not aligned, and a position displacement as half of the slot pitch is considered. Hence, the flux linkage is concentrated to increase the power factor. The configuration of the spoke-type linear machine is depicted in Figure 19. However, the power factor equals 0.40, which is still a low value.

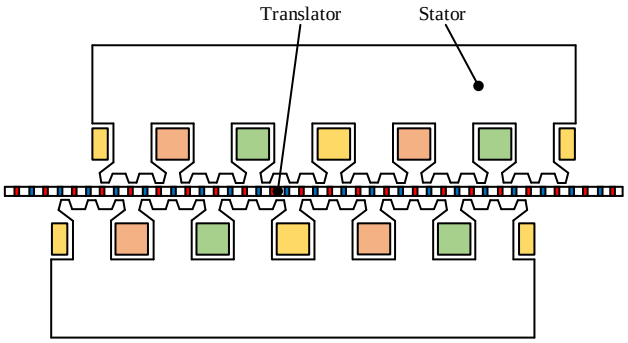

Figure 19. A dual-stator spoke-type linear vernier machine (DSSLVM).

5.2.3. High-Temperature Superconducting (HTS) Bulks

The power factor and power density of linear PM vernier generators can be significantly developed by adopting High-temperature superconducting (HTS) bulks. The relative permeability of HTS bulks is approximately equal to zero for the case that operation temperature does not exceed the critical temperature based on the Meissner effect [115]. Hence, the leakage flux is shielded, which results in the increment of the flux linkage and improving the power factor and power density [116]. A direct current (DC) is applied to the HTS bulks, and the airgap flux density can be controlled by adjusting the current [117]. A linear PM vernier generator fed by an additional DC excitation undergoes two separate flux paths, namely the flux produced by PMs and flux generated by the additional DC field windings. The DC excitation can be regulated to raise the airgap flux density when the flux of PMs and the flux excited by the DC field are aligned in the same direction [118].

In order to further improve the operation of the dual-stator spoke-type linear vernier machine (DSSLVM), shown in Figure 19, a novel structure equipped with high temperature superconducting (HTS) bulks was proposed in [119]. The configuration of the HTS dual-stator spoke-type linear vernier machine (HTS-DSSLVM) is depicted in Figure 20, in which HTS bulks of yttrium boron copper oxide (YBCO) are located inside the flux modulation poles. The HTS-DSSLVM has a power factor of 0.60, which is improved compared to the DSSLVM. However, the equivalent airgap lengths of the HTS LPMVM are not the same owing to inserting HTS bulks inside the FMPs, leading to a higher detent force.

Despite the capability of increasing the power factor by adjusting a DC excitation, some concerns have inevitably arisen. The efficiency is influenced, and the temperature is increased [120]; thus, a cooling system is required [121,122]. Due to the movement of the translator used in wave energy applications, using the cooling system imposes more complexity and increases costs. A soft tube was exploited in [123] to connect the cooling system and pipes in a linear PM vernier generator, possessing the ability to be compressed by the movement of the translator. As a result, the weight increases, which is a negative point, particularly for wave energy extraction systems.

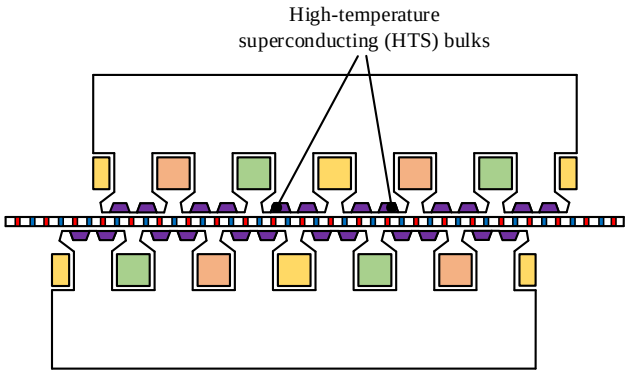

Figure 20. A HTS dual-stator spoke-type linear vernier machine (HTS-DSSLVM).

5.3. Thrust Force Ripple Reduction

In order to take advantage of a smooth operation and eradicate the mechanical vibrations and acoustic noise, linear vernier machines with low thrust force ripple are needed. The thrust force ripple can be calculated by using the following relationship:

$$\%F_{ripple} = \frac{F_{max} - F_{min}}{F_{avg}} \times 100 \tag{11}$$

where F_{max} is the maximum of thrust force, F_{min} is the minimum of thrust force, and F_{avg} is the average thrust force. The fundamental sources of thrust force ripple in linear PM vernier structures can be itemized as follows [124]:

- linear longitudinal end effect;
- cogging force;
- normal force in the perpendicular direction of reciprocation;
- non-sinusoidal back-EMF.

5.3.1. Linear Longitudinal End Effect

The longitudinal end effect of linear machines leads to a high thrust force ripple. As aforementioned, the linear concept is derived from the rotational structure (as shown in Figure 4), in which two open ends cause the flux passing through the ends not to have a closed magnetic circuit, unlike rotational counterparts. Certainly, the magnetic paths are not symmetric in linear vernier structures. The coils of the end slots generate the flux linkage with different amplitudes compared to other coils. Therefore, the linear structures inherently suffer from the longitudinal end effect, and they are expected to have a higher thrust force ripple [125].

5.3.2. Cogging Force

The undesired cogging force is caused by the slot effect of machines that employ permanent magnets, which can be defined as the tendency of translator PMs and stator teeth to be aligned in a position to have minimum reluctance. The cogging force and end force cause the detent force in linear PM vernier machines, which results in vibration and noise, decreasing the accuracy of positioning, and complicating the characteristics of the controlling system [126].

In order to diminish the adverse impact of detent force, the design characteristics of linear PM vernier generators can be optimized. Another effective method is selecting a proper combination of slots and poles for linear PM vernier generators. The cogging force period can be calculated for linear PM machines and is proportional to the inverse of its fundamental amplitude [127].

$$T_{cogging} \propto \frac{1}{LCM(2Z_r, Z_s)} \tag{12}$$

where $T_{cogging}$ is the cogging force period, and LCM is the lowest common multiple. Accordingly, it can be concluded that the higher $LCM(2Z_r, Z_s)$ results in a lower cogging force. Furthermore, the type of slots can be altered to offer a low cogging force. However, in linear PM vernier structures, the impact of slot type on the modulation must be considered into account to avoid the attenuation of the magnetic gearing effect.

5.3.3. Normal Force

The destructive normal (attraction) force of single-sided linear PM vernier machines is another substantial element that causes a high force ripple. An applicable method to reduce the normal force is adopting double-sided structures rather than single-sided counterparts. Hence, the force that exists in the vertical direction of reciprocating motion is diminished. In addition, the supporting system of the double-sided linear generator must be designed and assembled delicately to maintain a symmetrical configuration.

5.3.4. Non-Sinusoidal Back-EMF

The design procedure and analysis of electrical machines are carried out based on ideal back-EMF waveforms to obtain a smooth operation. Non-sinusoidal back-EMF is another element that generates a high thrust force ripple of linear vernier machines. Therefore, a control strategy is demanded to feed the linear vernier machines with sinusoidal back-EMF waveforms and avoid a high thrust force ripple. Furthermore, the harmonics of the current must be regarded into account from the viewpoint of the controller [124].

5.4. Cost Reduction

Linear PM machines are rather costly compared to linear structures without magnets. Reducing the cost of linear PM vernier generators used in wave energy applications is a significant issue, particularly for industrial projects on a large scale. Consequently, the cost reduction of linear vernier machines is an exciting subject to propose cost-effective structures.

The cost of energy (CE) can be defined as the ratio of the total cost to the total produced energy [128], as follows:

$$CE = \frac{Total\ Cost}{Total\ Produced\ Energy} \tag{13}$$

Total costs of electrical machines generally include initial capital costs and operational costs, and the relationship of the cost of energy (CE) can be rewritten:

$$CE = \frac{Initial\ Capital\ Costs + Operational\ Costs}{Power \times \eta} \tag{14}$$

where η is the efficiency of the electrical machine. Generally, the operational costs of brushless linear PM structures are less than their initial costs, mainly due to the consumption of PMs.

The cost of a power converter is linearly proportional to the kVA rating, which can be included in the following expression:

$$CE = \frac{A \times PM\ Volume + B \times 1/power\ factor}{\eta} \tag{15}$$

where A is the coefficient defined by the volume of consumed permanent magnets, and B is the cost coefficient related to the power converter. Therefore, an effective approach to decrease the costs is consuming less volume of PMs [129]. By employing hybrid configurations of linear vernier machines, the costs can be decreased, in which the magnets and armature windings can be adopted for the shorter side. Moreover, the cost of energy is inversely proportional to the power factor and efficiency of the linear vernier machine. In other words, by improving the power factor and efficiency of the linear vernier structure, the costs can be reduced [128].

In order to present a comprehensive comparison among different linear vernier machines, the classifications and outstanding merits and demerits of the linear generators are compared in Table 1. Overall, the most considerable advantage of linear vernier generators is their high force capability. The double-sided structure is preferred in some configurations to further increase the force capability. Moreover, using the structures with the flux focusing effect is also a practical approach to obtaining a high force density at low speeds. Nevertheless, the low power factor is a critical issue in vernier configurations, regarded as their most significant downside. Even though practical methods are proposed in [81,82,114] to increase their performance, the power factor values are reported as 0.44, 0.5, and 0.40, respectively. On the other hand, the power factor of a linear vernier machine was reported as high as 0.92 in [102], while the force density is also increased. However, there are still opportunities to improve the power factor and further increase the force density of vernier machines.

Table 1. A general comparison of different linear PM vernier generators.

Reference	Characteristics	Advantages	Disadvantages
Xiao et al. [26]	• Flat • Long translator • Double-sided • Surface-mounted • Distributed	• High force capability • Decreased flux leakage owing to utilization of HTS bulks • Low thrust force ripple	• Complicated structure • Requirement of cooling system
Botha et al. [71]	• Flat • Long translator (mover) • Single-sided • Surface-mounted/ Consequent-pole • Concentrated	• Study of airgap flux density analytical model • A quick analysis approach	• Ignoring saturation effect • Not modeling end effect
Baker et al. [81]	• Tubular • Long translator • Single-sided • Surface-mounted • Concentrated	• High force capability • Improved power factor • Mass saving	• Difficulty of prototyping • Still a low power factor
Baloch et al. [82]	• Tubular • Long translator • Double-sided • Spoke-type • Distributed	• High force capability • Improved flux linkage • Improved power factor	• Still a low power factor • Complicated structure • Uneconomical structure
Almoraya et al. [92]	• Flat • Long translator • Double-sided • Consequent-pole • Concentrated	• High force capability • Low thrust force ripple • Cost effective	• Estimated low power factor
Shi et al. [102]	• Flat • Long stator • Single-sided • Consequent-pole • Fractional pole	• High force capability • Low thrust force ripple • High power factor	• Low fault tolerance • Uneconomical structure due to PMs on the long side

Table 1. *Cont.*

Reference	Characteristics	Advantages	Disadvantages
Zhang et al. [104]	• Flat • Long stator • Double-sided • Surface-mounted • Toroidal	• High force capability	• Uneconomical structure • High thrust force ripple
Khaliq et al. [114]	• Flat • Long translator • Double-sided • Spoke-type • Distributed	• High force capability • Improved flux linkage owing to adopting flux focusing effect • Low thrust force ripple	• Low power factor
Baloch et al. [119]	• Flat • Long translator • Double-sided • Spoke-type • Distributed	• High force capability • Improved power factor	• High thrust force ripple • Uneconomical structure
Ching et al. [120]	• Flat • Long stator • Single-sided • Surface-mounted • Concentrated	• High force capability • Improved power factor	• High copper losses • Complicated structure
Du et al. [123]	• Flat • Long translator • Double-sided • Surface-mounted • Distributed	• High power density • Low cogging force • Low thrust force ripple	• Requirement of cooling system • Uneconomical structure

6. Analysis and Comparison of Different Linear PM Vernier Generators

In this section, some of the most functional structures of linear PM vernier generators used in wave energy conversion systems are compared to provide a comprehensive investigation. Two-dimensional finite element analysis (2D-FEA) is employed to analyze the electromagnetic behavior of four different linear PM vernier generators based on a system of Maxwell's equations. The outstanding linear vernier machines are selected as case studies to examine their capabilities to be used in wave energy applications. In order to define the boundary conditions, the magnetic vector potential of the outer region is set to be zero based on the Dirichlet boundary conditions. In addition, the non-linear characteristics of the translator and stator cores, the longitudinal end effect, and the leakage flux are considered into account, and the eddy current of permanent magnets is neglected.

A direct-drive linear primary PM vernier machine (LPPMVM) was proposed in [130], designed for wave energy applications. The LPPMVM exploits the single-sided structure, and both armature windings and PMs are located on the stator; therefore, the proposed structure is more robust and thermally stable. The configuration of the single-sided generator is depicted in Figure 21.

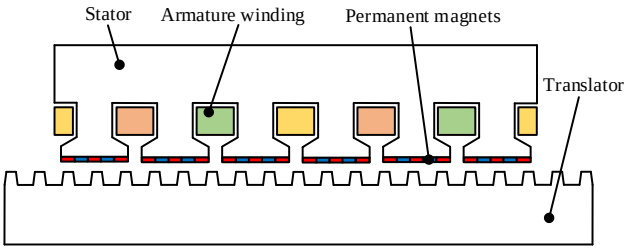

Figure 21. A single-sided linear primary PM vernier generator (LPPMVM).

The structure and operation principles of the single-sided generator have been studied in [130]. In addition, by considering the saturation effect, a magnetic equivalent circuit (MEC) method was proposed in [131].

The slot/pole combination of the single-sided LPPMVM is selected based on (17) to obtain the magnetic gearing effect. The single-sided linear machine possesses 6 primary teeth, and 5 PMs are located on each of the stator teeth. In addition, the armature winding is distributed to form 2 poles, and the proposed structure has a gear ratio of 17. As aforementioned, the performance of vernier structures is influenced by the gear ratio, in which a high force density and a low power factor can be estimated for the LPPMVM compared to similar structures with lower gear ratios. The most considerable advantage of the single-sided LPPMVM is offering a high thrust force density of 1.61 kN at the speed of 1 m/s. The thrust force density and the average thrust force per PM volume are 283 kN/m^3 and 13.4 N/cm^3, respectively.

Different structures have been developed based on the LPPMVM proposed in [130]. A linear stator spoke-type permanent magnet vernier machine (LSSPMVM) was proposed in [132] with similar topology and identical operation principles as LPPMVM. In order to decrease the leakage flux of the linear generator, surface-mounted PMs are replaced by spoke-type magnets, and a non-magnetic space is inserted between magnets and stator. A 2D schematic of the LSSPMVM with non-magnetic space is depicted in Figure 22.

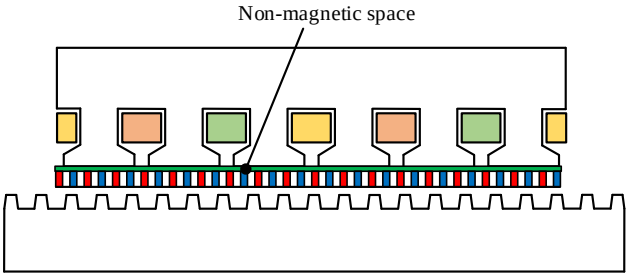

Figure 22. A linear stator spoke-type permanent magnet vernier machine (LSSPMVM) with non-magnetic space.

The magnetic flux distributions of the LSSPMVM with and without non-magnetic space are illustrated in Figure 23. As can be seen, adopting the non-magnetic space is an effective approach to decreasing the leakage flux, and the LSSPMVM with non-magnetic space has a lower amount of the leakage flux.

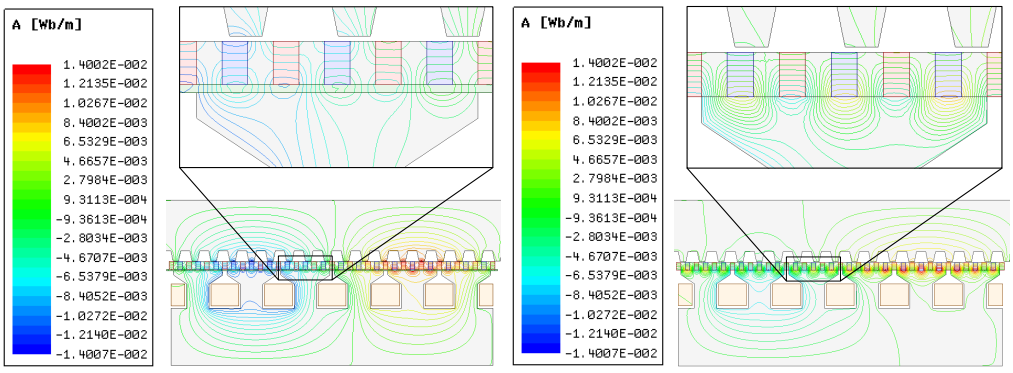

(**a**) (**b**)

Figure 23. Magnetic flux distribution of (**a**) LSSPMVM with non-magnetic space, and (**b**) LSSPMVM without non-magnetic space.

Figure 24 compares the flux linkage waveforms of LPPMVM and LSSPMVM with non-magnetic space, showing higher values for the LSSPMVM. The maximum amplitude

of the flux linkage is improved by approximately 58% for the case of using spoke-type magnets and adopting non-magnetic space.

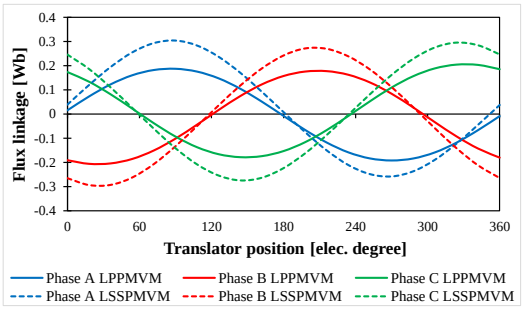

Figure 24. Flux linkage of LPPMVM and LSSPMVM with non-magnetic space.

Airgap flux density and harmonic spectra of the LPPMVM and LSSPMVM are illustrated in Figure 25. The amplitude of the 18th harmonic order is 0.79 T for the LSSPMVM and 0.68 *T* for the LPPMVM, which is improved by 16%. Adopting the non-magnetic space has resulted in the improvement of the airgap flux density. On the other hand, although the LSSPMVM has a higher volume of PMs than LPPMVM, the effectiveness of using the non-magnetic space was validated in [132] in comparison with a similar structure using the same volume of PMs.

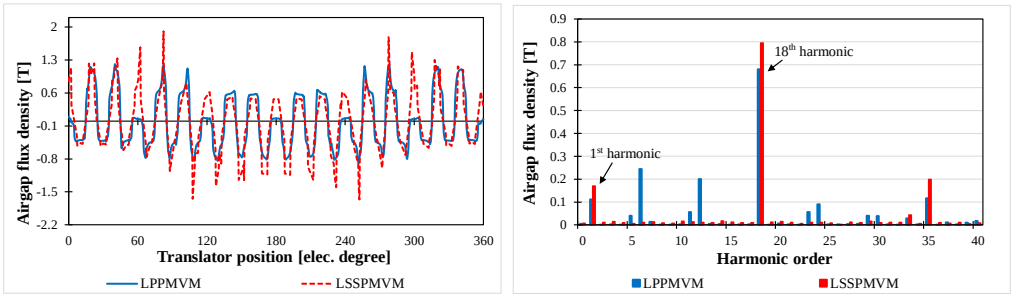

(**a**) (**b**)

Figure 25. Airgap flux density of LPPMVM and LSSPMVM, (**a**) Waveform and (**b**) Harmonic spectra.

The LSSPMVM with non-magnetic space offers an average thrust force of 2.18 kN, and the thrust force density equals 327 kN/m^3. By exploiting spoke-type PMs and the non-magnetic space, thrust force density is improved by 15.5% compared to the surface-mounted LPPMVM. Furthermore, both structures have low values of detent force, lower than 2% of the average thrust force. However, the LPPMVM and LSSPMVM have low power factor values of 0.26 and 0.27, respectively.

Two topologies of linear PM vernier generators employing inset magnet consequent pole (IMCP) and V-shaped consequent pole (VCP) structures have been proposed in [133]. The configurations of linear vernier generators are depicted in Figure 26. As can be seen, the consequent pole structures are preferred for both linear machines with different magnet types to decrease the leakage flux.

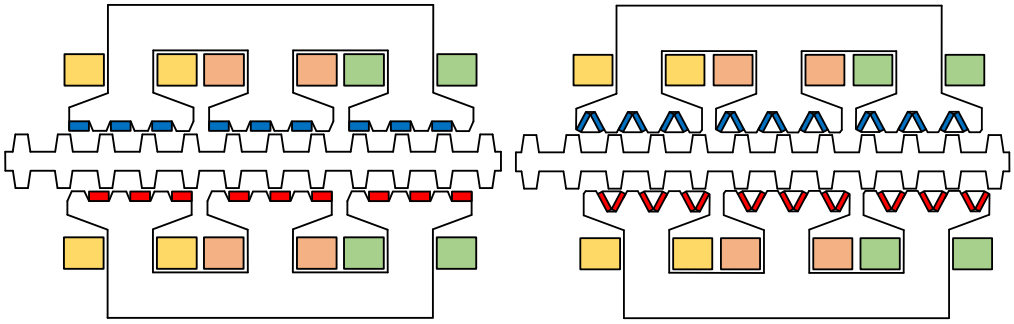

(**a**) (**b**)

Figure 26. (**a**) Inset magnet consequent pole (IMCP), and (**b**) V-shaped consequent pole (VCP) linear vernier generators.

The IMCP vernier generator possesses a double-sided E-core stator, and each stator tooth adopts three magnets. The proposed IMCP machine has 9 PM pole pairs, 1 armature winding pole pair, and 10 translator teeth. Accordingly, the magnetic gearing effect can be obtained, and a high force capability is estimated for the linear vernier structure. The flux distribution of the IMCP vernier generator at different positions of the translator is shown in Figure 27. As can be seen, a short displacement of the translator provides a considerable change in the flux distribution, resulting from the magnetic gearing effect. Hence, the linear vernier machine has a high thrust force density.

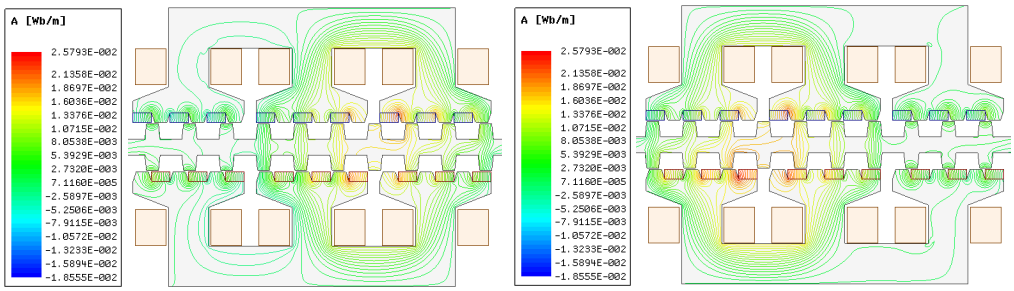

(**a**) (**b**)

Figure 27. The flux distribution of the IMCP vernier generator at different positions of the translator: (**a**) displacement = 0 mm, (**b**) displacement = 8 mm.

The V-type structure is another practical choice for obtaining the flux focusing effect and increasing the flux linkage. As shown in Figure 26b, the iron bridges of the V-type configuration are eliminated in order to further decrease the leakage flux. Average thrust force values of IMCP and V-type linear vernier generators are reported as 739 N and 812 N, respectively. In addition, the thrust force density is 354 kN/m^3 for the IMCP machine and 389 kN/m^3 for the VCP machine. The linear vernier generator with the VCP structure has 10% higher thrust force density than the IMCP counterpart. Furthermore, the linear generator with VCP magnets has a higher power factor of 0.65 compared to 0.51 for the IMCP counterpart. Figure 28 shows the flux linkage waveforms of the IMCP and VCP LPMVMs. The maximum flux linkage values of phase A are reported as 0.14 Wb and 0.18 Wb for the IMCP and VCP machines, respectively. The higher flux linkage of the VCP linear vernier structure results from the unique configuration of V-type magnets and the flux focusing effect.

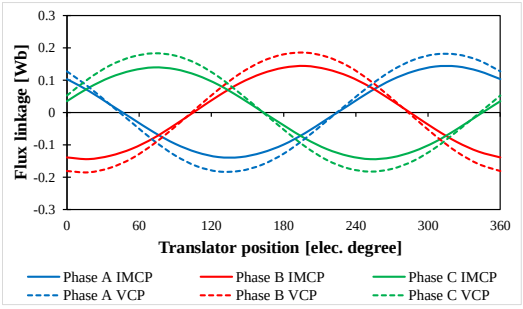

Figure 28. Flux linkage of IMCP and VCP LPMVMs.

The detent force of IMCP and VCP linear machines are compared in Figure 29. The peak to peak values are reported as 59 N and 48 N for the IMCP and VCP LPMVMs, respectively. The linear structure with V-type magnets has a lower detent force and excels the IMCP machine in terms of the low force ripple.

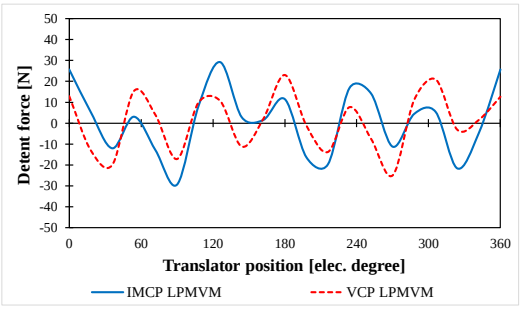

Figure 29. Detent force comparison of IMCP and VCP LPMVMs.

The temperature rise of different parts affects the performance and lifetime of the linear generators. Consequently, thermal analysis is regarded as one of the principal steps in the evaluation procedure of linear machines used in wave energy systems. The finite element analysis thermal modeling is exploited to thermally analyze the linear machines and provide a reliable analysis. The ambient temperature is assumed to be 23 °C (296.15 K) to provide an accurate operational condition. In addition, the thermal properties of the materials are presented in Table 2.

Table 2. Thermal characteristics of the materials [134].

Material	Thermal Conductivity [W/(m·K)]	Specific Heat Capacity [J/(kg·K)]	Density [kg/m^3]
Steel	30	460	7650
Magnet	7.6	460	7500
Copper	401	385	8933

Once the electromagnetic behavior analysis of the linear generators is realized, the thermal field analysis can be performed. The core and copper losses of linear PM vernier machines are regarded as heat sources. The copper loss model is obtained based on the resistive heating, and the equation of the model is assumed to be:

$$P_{cu} = \frac{1}{T}\int_{T_{end}}^{T_{end}-T} J \cdot E dt \tag{16}$$

where T is the electrical period, T_{end} is the end time, J is the current density, and E is the electric field. Furthermore, the Bertotti loss model is exploited to accurately characterize

the hysteresis, eddy current, and excess losses in linear vernier generators. The Bertotti loss model can be defined as:

$$P_{fe} = k_h f B_{gmax}^{\beta} + k_c f^2 B_{gmax}^2 + k_e f^{1.5} B_{gmax}^{1.5} \quad (17)$$

where k_h is the hysteresis loss coefficient, β is Steinmetz constant, k_c is the eddy current loss coefficient, and k_e is the excess loss coefficient [135–137]. The losses are calculated through the utilization of finite element analysis. The LSSPMVM possesses the maximum core loss, reported as 61.5 W. The core losses of LPPMVM, IMCP LPMVM, and VCP LPMVM are 44.4 W, 18.4 W, and 22.0 W, respectively. The volumetric loss density for the linear PM vernier generators is shown in Figure 30.

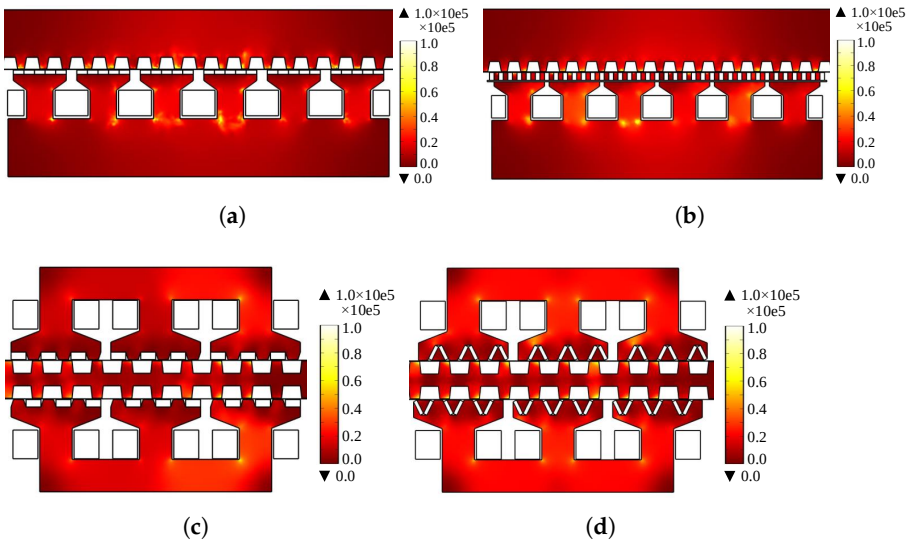

Figure 30. Volumetric loss density [W/m^3] of linear machines: (**a**) LPPMVM, (**b**) LSSPMVM, (**c**) IMCP LPMVM, and (**d**) VCP LPMVM.

The heat sources lead to the temperature increment of linear machines; therefore, the losses calculated in the electromagnetic analysis are used to survey the thermal behavior. Defining heat transfer mechanisms is an important stage in thermal analysis. Conduction and convection mechanisms are applied for the thermal analysis of the linear machines in this section, while the radiation is neglected. Heat transfer coefficients (HTCs) have been calculated through the use of empirical expressions to accurately model the thermal behavior. The linear machines operate under natural cooling convection. Finally, a commercial software package based on finite element analysis is exploited to estimate the temperature rise of different parts by applying the heat sources and boundary conditions. The process ends when the simulation is converged. The temperature rise of the stators is shown in Figure 31 during 6 h of the simulation process. The LSSPMVM undergoes the maximum temperature rise of the stator among the case studies, in which the stator temperature rises to reach the maximum temperature of 347 K. The maximum temperature is below the Curie temperature of magnets, and the temperature rise can not significantly influence the performance of the linear machines. On the other hand, the IMCP LPMVM has the minimum temperature rise owing to the lower losses.

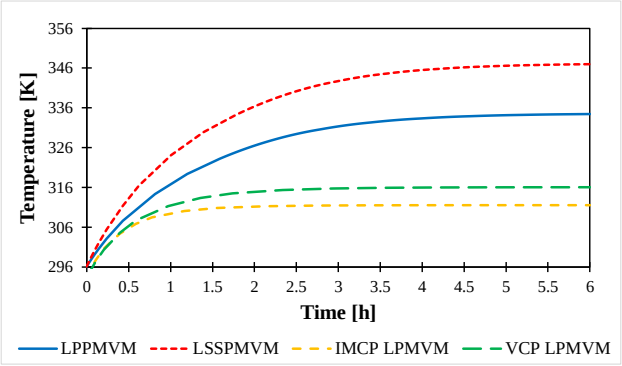

Figure 31. Temperature rise of the stator of linear generators.

The IMCP and VCP LPMVMs are more advantageous than LPPMVM and LSSPMVM in terms of higher efficiencies. The efficiency values are reported as 84.8%, 87.8 %, 91.6%, and 92.0% for LPPMVM, LSSPMVM, IMCP LPMVM, and VCP LPMVM, respectively. The information on copper losses, core losses, and efficiencies of the linear generators are briefed in Table 3.

Table 3. Characteristics of different linear PM vernier generators.

	LPPMVM [130]	**LSSPMVM [132]**	**IMCP LPMVM [133]**	**VCP LPMVM [133]**
Structure	Flat	Flat	Flat	Flat
Single/double-sided	Single-sided	Single-sided	Double-sided	Double-sided
Armature winding type	Distributed	Distributed	Concentrated	Concentrated
PM type	Surface-mounted	Spoke-type	Consequent pole	V-type
Location of PMs	Stator	Stator	Stator	Stator
No. of PM pole pairs	18	18	9	9
No. of winding pole pairs	1	1	1	1
No. of translator teeth	17	17	10	10
Gear ratio	17	17	10	10
No. of PMs per stator tooth	5	5	3	6
Frequency [Hz]	50	50	50	50
No. of phases	3	3	3	3
PM volume [cm^3]	120	150	64.8	64.8
Magnet remanence [T]	1.2	1.2	1.24	1.24
Active length [mm]	360	360	232	232
Thickness of linear machine [mm]	158	185	180	180
Stack length [mm]	100	100	50	50
Translator tooth pitch [mm]	21.17	21.17	24	24
Stator tooth pitch [mm]	60	60	80	80
Airgap length [mm]	1	1	1	1
Rated speed [m/s]	1	1	1.2	1.2
No. of winding turns per phase	142	140	90	90
Current density [A/mm^2]	4.3	4.3	3.5	3.5
No-load back-EMF [V]	60	87	45	57
Flux linkage [Wb]	0.19	0.30	0.14	0.18
Average thrust force [kN]	1.61	2.18	0.739	0.812
Thrust force density [kN/m^3]	283	327	354	389
Force/PM volume [N/cm^3]	13.4	14.5	11.1	12.5
Power factor	0.26	0.27	0.51	0.65
Copper loss [W]	243.5	240.1	62.6	62.6
Core loss [W]	44.4	61.5	18.4	22.0
Efficiency [%]	84.8	87.8	91.6	92.0
Detent force pk2pk [N]	31 (1.9%)	36 (1.65%)	59 (7.9%)	48 (5.9 %)
Thrust force pk2pk [N]	50	93	66	51
Thrust force ripple [%]	3.1	4.2	8.9	6.2

To conclude, the thrust force of four linear generators is illustrated in Figure 32 to make a comparison based on their force capabilities. However, due to the different dimensions and features of electrical machines, average force per volume is regarded as a relatively logical indicator to compare the force capabilities. Thrust force density of LPPMVM, LSSPMVM, IMCP LPMVM, and VCP LPMVM are reported 283 kN/m^3, 327 kN/m^3, 354 kN/m^3, and 389 kN/m^3, respectively. The VCP linear vernier machine offers the highest force density and also the highest power factor. The power factor of the VCP LPMVM is 0.65, which is improved compared to the IMCP counterpart owing to the flux focusing effect. Another significant criterion is the effective usage of PMs, in which the average force per PM volume of LSSPMVM equals 14.5 N/cm^3, known as the highest value among the four machines. Moreover, the linear machines have low detent force and force ripple values. The LPPMVM has the minimum thrust force ripple, reported as 3.1%. A fair comparison can be carried out by considering different elements that influence the performance of linear machines. The characteristics of the LPPMVM, LSSPMVM with non-magnetic space, IMCP LPMVM, and VCP LPMVM are tabulated in Table 3. Generally, vernier structures are suitable candidates for wave energy applications due to their high force capability. Moreover, their low power factor can be enhanced by using practical strategies.

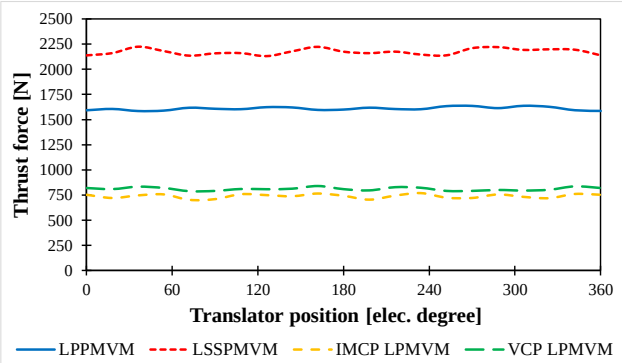

Figure 32. Thrust force of linear generators.

The results obtained from FEA show a negligible difference between the simulation results and experimental results obtained from the main references. The difference arises inevitably from using FEA software packages, applying operational conditions, the meshing, and other elements considered by the designers. The analysis in this paper validates the characteristics of the linear vernier machines and confirms the advantages of the proposed structures for wave energy harvesting systems.

7. Conclusions and Outlooks

Linear PM vernier machines are excellent choices to offer high power/force densities at low speeds. Consequently, linear vernier generators are practical candidates for wave energy applications. In this paper, a comprehensive study on different linear vernier structures has been carried out. Different linear vernier machines have been categorized, and their operation principles are evaluated and compared with other structures. Furthermore, different approaches to improve the performance of linear vernier structures are classified and surveyed. Finally, some practical linear vernier generators have been selected to analyze their performance using 2D-FEA. The results validated the outstanding merit of the high force density of vernier machines, making them beneficial options for harvesting wave energy.

Overall, linear vernier structures investigated as case studies offer a high force density. The LPPMVM is an excellent candidate for wave energy systems in terms of offering the high capability of thrust force. By adopting the non-magnetic space, the LSSPMVM is proposed to decrease the leakage flux. Accordingly, the thrust force density is improved

by 15.5% compared to the LPPMVM. However, both structures have a low power factor, necessitating high rating converters. The IMCP and VCP linear vernier machines have been studied by using 2D-FEA, possessing higher values of power factor and thrust force density. The VCP LPMVM provides 10% and 19% higher force density in comparison with the IMCP machine and LSSPMVM, respectively. Even though the VCP machine has a higher force ripple than the LPPMVM and LSSPMVM, the advantages of high force density and higher power factor outweigh its relatively higher force ripple. The thrust force ripple values of LPPMVM and LSSPMVM are lower than the VCP linear generator; however, the difference cannot make a considerable change. Consequently, the VCP structure can be regarded as a functional configuration to be employed in wave energy systems.

Also, the following outlooks can be conducted in order to further improve the performance of linear PM vernier machines:

- The most considerable disadvantage of linear PM vernier machines is their poor power factor. Innovative techniques are required to further develop the low power factor of linear vernier structures.
- Due to the time-consuming process of analyzing linear PM vernier generators based on FEA, accurate analytical methods are desired to provide analysis models in a short time.
- One of the most important criteria that must be considered into account is the cost of linear PM vernier generators, which are required to be declined by offering more economically viable structures and the decrease of the volume of magnets.
- The reduction of the weight of linear PM vernier generators can be realized by reducing the active material. There are opportunities to employ more lightweight linear generators for wave energy harvesting systems.
- Unconventional topologies can be introduced to improve the performance of linear vernier generators and facilitate their utilization in wave energy applications.
- The unwanted longitudinal end effect of linear PM vernier generators imposes a disadvantageous impact on the machine performance, which is desired to be diminished.
- Thermal analysis of linear PM vernier generators is another interesting subject in which not enough research has been accomplished so far.
- The magnetic gear ratio significantly affects the performance of linear PM vernier generators used in wave energy applications. Analytical and numerical methods are required to investigate the optimal gear ratio values.
- The configuration and number of flux modulation poles can have an impact on the gear ratio and the machine performance, which can be surveyed for linear vernier structures.
- A system-level optimization process is needed to improve the efficiency and performance of a linear vernier generator used in wave energy applications.
- Linear PM vernier machines utilize more number of PMs compared to linear PM synchronous machines; thus, the study on the possibilities to avoid irreversible demagnetization can be very useful.

Author Contributions: Conceptualisation, R.J., P.A., M.A., M.M.D.; methodology, R.J., P.A., M.A., M.M.D.; primary research, R.J.; secondary research, R.J., P.A., M.A., M.M.D.; formal analysis, R.J., P.A., M.A., M.M.D.; writing—original draft preparation, R.J.; writing—review and editing, P.A., M.A., M.M.D.; supervision, P.A., M.A., M.M.D.; project administration, P.A. All authors have read and agreed to the published version of the manuscript.

Funding: This research received no external funding.

Institutional Review Board Statement: Not applicable.

Informed Consent Statement: Not applicable.

Data Availability Statement: The data that supports the findings of this study are available within the article.

Conflicts of Interest: The authors declare no conflict of interest.

Abbreviations

AWS	Archimedes wave swing
CPHPM	Consequent-pole and Halbach permanent magnet
DC	Direct current
DSSLVM	Dual-stator spoke-type linear vernier machine
DSTVM	Dual stator tubular vernier machine
EMF	Electromotive force
EMN	Equivalent magnetic network
FEA	Finite element analysis
FMP	Flux modulation pole
FP	Fractional pole
GCD	Greatest common divisor
GR	Gear ratio
HTS	High temperature superconducting
IMCP	Inset magnet consequent pole
LCM	Lowest common multiple
LCPSPMVM	Linear consequent pole stator permanent magnet vernier machine
LPMSG	Linear permanent magnet synchronous generator
LPMSM	Linear permanent magnet synchronous machine
LPMVG	Linear permanent magnet vernier generator
LPMVM	Linear permanent magnet vernier machine
LPPMVM	Linear primary PM vernier machine
LSSPMVM	Linear stator spoke-type permanent magnet vernier machine
MEC	Magnetic equivalent circuit
MMF	Magnetomotive force
NdFeB	Neodymium–iron–boron
PM	Permanent magnet
PTO	Power take-off
VCP	V-shaped consequent pole
WEC	Wave energy converter
YBCO	Yttrium boron copper oxide
A	Coefficient defined by the volume of PMs
B	Cost coefficient related to the power converter
B_{gmax}	Maximum flux density
CE	Cost of energy
E	Electric field
F_{avg}	Average thrust force
F_{max}	Maximum of thrust force
F_{min}	Minimum of thrust force
I	Current
J	Current density
k_c	Eddy current loss coefficient
k_d	Flux leakage coefficient
k_e	Excess loss coefficient
k_h	Hysteresis loss coefficient
k_s	Electric loading
k_w	Winding factor
L	Effective length
L_s	Synchronous inductance
L_{stk}	Stack length
m	Number of phases
P	Electromagnetic power
p	Number of stator armture winding pole pairs
R_{ag1}	Airgap reluctance of the slot
R_{ag2}	Airgap reluctance of the tooth
R_m	Reluctance of the magne
T	Electrical period

$T_{cogging}$	Cogging force period
T_{end}	End time
v	Mechanical speed of the moving part
v_{eff}	Mechanical speed of the effective flux
Z_r	Number of translator pole pairs
Z_s	Number of stator teeth
β	Steinmetz constant
η	Efficiency of the electrical machine
τ_{eff}	Effective flux pitch
τ_{eff}	Tooth pitch of the mover
ϕ_1	Leakage flux of surface-mounted structure
ϕ_2	Leakage flux of consequent-pole structure
Ψ_{PM}	Flux linkage produced by PMs

References

1. Shi, C.; Qu, R.; Li, D.; Gao, Y.; Li, R. Comparative study on a novel consequent-pole modular linear vernier machine with PMs on both mover and stator iron cores. In Proceedings of the 2019 IEEE Energy Conversion Congress and Exposition (ECCE), Baltimore, MD, USA, 29 September–3 October 2019; IEEE: Piscataway, NJ, USA, 2019; pp. 712–716.
2. Souissi, A.; Abdennadher, I.; Masmoudi, A. *Linear Synchronous Machines: Application to Sustainable Energy and Mobility*; Springer: Berlin/Heidelberg, Germany, 2019.
3. Shen, Y.; Kang, M.; Ji, J.; Zhao, W.; Liu, G. Design and analysis of a novel modular six-phase linear permanent-magnet vernier machine. In Proceedings of the 2017 20th International Conference on Electrical Machines and Systems (ICEMS), Sydney, Australia, 11–14 August 2017; IEEE: Piscataway, NJ, USA, 2017; pp. 1–5.
4. Fan, H.; Chau, K.; Liu, C.; Cao, L.; Ching, T. Quantitative comparison of novel dual-PM linear motors for ropeless elevator system. *IEEE Trans. Magn.* **2018**, *54*, 1–6.
5. Xu, X.; Sun, Z.; Du, B.; Ai, L. Pole optimization and thrust ripple suppression of new Halbach consequent-pole PMLSM for ropeless elevator propulsion. *IEEE Access* **2020**, *8*, 62042–62052. [CrossRef]
6. Kameda, D.; Hirata, K.; Niguchi, N. Study of linear vernier motor for household automatic doors. In Proceedings of the 2017 11th International Symposium on Linear Drives for Industry Applications (LDIA), Osaka, Japan, 6–8 September 2017; IEEE: Piscataway, NJ, USA, 2017; pp. 1–4.
7. Duong, M.T.; Chun, Y.D. Optimal design of a novel exterior permanent magnet tubular machine for energy harvesting from vehicle suspension system. *IEEE Trans. Energy Convers.* **2020**, *35*, 1772–1780. [CrossRef]
8. Hu, Y.; Xu, Z.; Yang, L.; Liu, L. Electromagnetic Loss Analysis of a Linear Motor System Designed for a Free-Piston Engine Generator. *Electronics* **2020**, *9*, 621. [CrossRef]
9. Yang, L.; Xu, Z.; Liu, L.; Liu, N.; Yu, H. A tubular PM linear generator with a coreless moving-coil for free-piston engines. *IEEE Trans. Energy Convers.* **2019**, *34*, 1309–1316. [CrossRef]
10. Molla, S.; Farrok, O.; Islam, M.R.; Xu, W. The novel low reluctance superconducting permanent magnet linear generator for oceanic wave energy extraction. *IEEE Trans. Appl. Supercond.* **2021**, *31*, 1–5. [CrossRef]
11. Rusu, E.; Onea, F. A review of the technologies for wave energy extraction. *Clean Energy* **2018**, *2*, 10–19. [CrossRef]
12. Amini, E.; Asadi, R.; Golbaz, D.; Nasiri, M.; Naeeni, S.T.O.; Majidi Nezhad, M.; Piras, G.; Neshat, M. Comparative study of oscillating surge wave energy converter performance: A case study for southern coasts of the Caspian sea. *Sustainability* **2021**, *13*, 10932. [CrossRef]
13. Vining, J.G.; Muetze, A. Economic factors and incentives for ocean wave energy conversion. *IEEE Trans. Ind. Appl.* **2009**, *45*, 547–554. [CrossRef]
14. Derakhshani, M.M.; Ardebili, M.; Jafari, R. A survey on a novel double-rotor spoke-type permanent magnet induction generator employing bridged and bridgeless structures. *Electr. Eng.* **2021**, *104*, 899–911. [CrossRef]
15. Lyden, S.; Haque, M.E. Modelling, parameter estimation and assessment of partial shading conditions of photovoltaic modules. *J. Mod. Power Syst. Clean Energy* **2019**, *7*, 55–64. [CrossRef]
16. Rabaia, M.K.H.; Abdelkareem, M.A.; Sayed, E.T.; Elsaid, K.; Chae, K.J.; Wilberforce, T.; Olabi, A. Environmental impacts of solar energy systems: A review. *Sci. Total Environ.* **2021**, *754*, 141989. [CrossRef] [PubMed]
17. Khatri, P.; Wang, X. Comprehensive review of a linear electrical generator for ocean wave energy conversion. *IET Renew. Power Gener.* **2020**, *14*, 949–958. [CrossRef]
18. Farrok, O.; Islam, M.R.; Muttaqi, K.M.; Sutanto, D.; Zhu, J. Design and optimization of a novel dual-port linear generator for oceanic wave energy conversion. *IEEE Trans. Ind. Electron.* **2019**, *67*, 3409–3418. [CrossRef]
19. Trapanese, M.; Boscaino, V.; Cipriani, G.; Curto, D.; Di Dio, V.; Franzitta, V. A permanent magnet linear generator for the enhancement of the reliability of a wave energy conversion system. *IEEE Trans. Ind. Electron.* **2018**, *66*, 4934–4944. [CrossRef]
20. Rahman, A.; Farrok, O.; Islam, M.R.; Xu, W. Recent progress in electrical generators for oceanic wave energy conversion. *IEEE Access* **2020**, *8*, 138595–138615. [CrossRef]
21. Du, Y.; Cheng, M.; Chau, K.; Liu, X.; Xiao, F.; Zhao, W.; Shi, K.; Mo, L. Comparison of linear primary permanent magnet vernier machine and linear vernier hybrid machine. *IEEE Trans. Magn.* **2014**, *50*, 1–4. [CrossRef]
22. Eriksson, S. Design of permanent-magnet linear generators with constant-torque-angle control for wave power. *Energies* **2019**, *12*, 1312. [CrossRef]

23. Sjölund, J.; Leijon, M.; Eriksson, S. Method for optimizing the magnetic circuit of a linear generator using FEM simulations. *AIP Adv.* **2020**, *10*, 035312. [CrossRef]
24. Eklund, P.; Eriksson, S. The influence of permanent magnet material properties on generator rotor design. *Energies* **2019**, *12*, 1314. [CrossRef]
25. Asef, P.; Perpi nà, R.B.; Lapthorn, A.C. Optimal pole number for magnetic noise reduction in variable-speed permanent magnet synchronous machines with fractional-slot concentrated windings. *IEEE Trans. Transp. Electrif.* **2018**, *5*, 126–134. [CrossRef]
26. Xiao, F.; Du, Y.; Wang, Y.; Chen, M.; Ching, T.; Liu, X. Modeling and analysis of a linear stator permanent-magnet vernier HTS machine. *IEEE Trans. Appl. Supercond.* **2014**, *25*, 1–4. [CrossRef]
27. Li, W.; Chau, K.; Li, J. Simulation of a tubular linear magnetic gear using HTS bulks for field modulation. *IEEE Trans. Appl. Supercond.* **2010**, *21*, 1167–1170. [CrossRef]
28. Li, W.; Chau, K.; Lee, C.H.; Ching, T.; Chen, M.; Jiang, J. A new linear magnetic gear with adjustable gear ratios and its application for direct-drive wave energy extraction. *Renew. Energy* **2017**, *105*, 199–208. [CrossRef]
29. Li, W.; Chau, K.; Jiang, J. Application of linear magnetic gears for pseudo-direct-drive oceanic wave energy harvesting. *IEEE Trans. Magn.* **2011**, *47*, 2624–2627. [CrossRef]
30. Faiz, J.; Amini-Valeshani, S.; Ghods, M. Design and performance of linear Vernier generators—The state of the art and case study. *Int. Trans. Electr. Energy Syst.* **2021**, *31*, e12723. [CrossRef]
31. Liu, G.; Zhong, H.; Xu, L.; Zhao, W. Analysis and evaluation of a linear primary permanent magnet vernier machine with multiharmonics. *IEEE Trans. Ind. Electron.* **2020**, *68*, 1982–1993. [CrossRef]
32. Sjölund, J.; Frost, A.E.; Leijon, M.; Eriksson, S. End effects and geometric compensation in linear permanent magnet synchronous generators with different topologies. *Designs* **2021**, *5*, 64. [CrossRef]
33. Derakhshani, M.M.; Ardebili, M.; Cheraghi, M.; Jafari, R. Investigation of structure and performance of a permanent magnet vernier induction generator for use in double-turbine wind systems in urban areas. *IET Renew. Power Gener.* **2020**, *14*, 4169–4178. [CrossRef]
34. Khezri, R.; Mahmoudi, A.; Aki, H. Optimal planning of solar photovoltaic and battery storage systems for grid-connected residential sector: Review, challenges and new perspectives. *Renew. Sustain. Energy Rev.* **2022**, *153*, 111763. [CrossRef]
35. Nam, J.W.; Sung, Y.J.; Cho, S.W. Effective Mooring Rope Tension in Mechanical and Hydraulic Power Take-Off of Wave Energy Converter. *Sustainability* **2021**, *13*, 9803. [CrossRef]
36. Vukajlovic, N.; Katie, V.; Milicevic, D.; Dumnic, B.; Popadic, B. Active control of induction generator in ocean wave energy conversion system. In Proceedings of the 2018 IEEE 18th International Power Electronics and Motion Control Conference (PEMC), Budapest, Hungary, 26–30 August 2018; IEEE: Piscataway, NJ, USA, 2018; pp. 324–329.
37. Drew, B.; Plummer, A.R.; Sahinkaya, M.N. A review of wave energy converter technology. *Proc. Inst. Mech. Eng. Part A J. Power Energy* **2009**, *223*, 887–902. [CrossRef]
38. Cornett, A.M. A global wave energy resource assessment. In Proceedings of the Eighteenth International Offshore and Polar Engineering Conference, Vancouver, BC, Canada, 6–11 July 2008; OnePetro: Richardson, TX, USA, 2008.
39. Ahamed, R.; McKee, K.; Howard, I. Advancements of wave energy converters based on power take off (PTO) systems: A review. *Ocean Eng.* **2020**, *204*, 107248. [CrossRef]
40. Brekken, T.K.; Von Jouanne, A.; Han, H.Y. Ocean wave energy overview and research at Oregon State University. In Proceedings of the 2009 IEEE Power Electronics and Machines in Wind Applications, Lincoln, NE, USA, 24–26 June 2009; IEEE: Piscataway, NJ, USA, 2009; pp. 1–7.
41. Aderinto, T.; Li, H. Ocean wave energy converters: Status and challenges. *Energies* **2018**, *11*, 1250. [CrossRef]
42. Haces-Fernandez, F.; Li, H.; Ramirez, D. Analysis of Wave Energy Behavior and Its Underlying Reasons in the Gulf of Mexico Based on Computer Animation and Energy Events Concept. *Sustainability* **2022**, *14*, 4687. [CrossRef]
43. Potapenko, T.; Burchell, J.; Eriksson, S.; Temiz, I. Wave Energy Converter's Slack and Stiff Connection: Study of Absorbed Power in Irregular Waves. *Energies* **2021**, *14*, 7892. [CrossRef]
44. Bosma, B.; Brekken, T.; Lomonaco, P.; DuPont, B.; Sharp, C.; Batten, B. Array modeling and testing of fixed OWC type Wave Energy Converters. *Int. Mar. Energy J.* **2020**, *3*, 137–143. [CrossRef]
45. Masoomi, M.; Yousefifard, M.; Mosavi, A. Efficiency Assessment of an Amended Oscillating Water Column Using OpenFOAM. *Sustainability* **2021**, *13*, 5633. [CrossRef]
46. Faiz, J.; Nematsaberi, A. Linear electrical generator topologies for direct-drive marine wave energy conversion—An overview. *IET Renew. Power Gener.* **2017**, *11*, 1163–1176. [CrossRef]
47. Nath, R.; Kankar, P.; Gupta, V. Study of Archimedes Wave Swing Harvester for Indian Ocean. In *Advanced Materials*; Springer: Berlin/Heidelberg, Germany, 2019; pp. 545–556.
48. So, R.; Bosma, B.; Ruehl, K.; Brekken, T.K. Modeling of a wave energy oscillating water column as a point absorber using wec-sim. *IEEE Trans. Sustain. Energy* **2019**, *11*, 851–858. [CrossRef]
49. Li, W.; Chau, K. Simulation of a linear permanent magnet vernier machine for direct-drive wave power generation. In Proceedings of the 2011 International Conference on Electrical Machines and Systems, Beijing, China, 20–23 August 2011; IEEE: Piscataway, NJ, USA, 2011; pp. 1–6.
50. Xi, R.; Zhang, H.; Zhao, H.; Mondal, R. High-performance and robust bistable point absorber wave energy converter. *Ocean Eng.* **2021**, *229*, 108767. [CrossRef]

51. Engström, J.; Kurupath, V.; Isberg, J.; Leijon, M. A resonant two body system for a point absorbing wave energy converter with direct-driven linear generator. *J. Appl. Phys.* **2011**, *110*, 124904. [CrossRef]
52. Al Shami, E.; Zhang, R.; Wang, X. Point absorber wave energy harvesters: A review of recent developments. *Energies* **2018**, *12*, 47. [CrossRef]
53. Pecher, A.; Kofoed, J.P. *Handbook of Ocean Wave Energy*; Springer Nature: Berlin/Heidelberg, Germany, 2017.
54. Ahamed, R.; McKee, K.; Howard, I. A Review of the Linear Generator Type of Wave Energy Converters' Power Take-Off Systems. *Sustainability* **2022**, *14*, 9936. [CrossRef]
55. McGilton, B.; Almoraya, A.A.; Raihan, R.; Crozier, R.; Baker, N.J.; Mueller, M. Investigation into linear generators with integrated magnetic gear for wave energy power take off. *J. Eng.* **2019**, *2019*, 5069–5072. [CrossRef]
56. Guo, K.; Guo, Y. Design optimization of linear-rotary motion permanent magnet generator with E-shaped stator. *IEEE Trans. Appl. Supercond.* **2021**, *31*, 1–5. [CrossRef]
57. Leijon, M.; Boström, C.; Danielsson, O.; Gustafsson, S.; Haikonen, K.; Langhamer, O.; Strömstedt, E.; Stålberg, M.; Sundberg, J.; Svensson, O.; et al. Wave energy from the North Sea: Experiences from the Lysekil research site. *Surv. Geophys.* **2008**, *29*, 221–240. [CrossRef]
58. Elwood, D.; Yim, S.C.; Prudell, J.; Stillinger, C.; Von Jouanne, A.; Brekken, T.; Brown, A.; Paasch, R. Design, construction, and ocean testing of a taut-moored dual-body wave energy converter with a linear generator power take-off. *Renew. Energy* **2010**, *35*, 348–354. [CrossRef]
59. Xu, W.; Islam, M.R.; Pucci, M. *Advanced Linear Machines and Drive Systems*; Springer: Berlin/Heidelberg, Germany, 2019.
60. Gardner, M.C.; Johnson, M.; Toliyat, H.A. Analysis of high gear ratio capabilities for single-stage, series multistage, and compound differential coaxial magnetic gears. *IEEE Trans. Energy Convers.* **2018**, *34*, 665–672. [CrossRef]
61. Gardner, M.C.; Praslicka, B.; Johnson, M.; Toliyat, H.A. Optimization of Coaxial Magnetic Gear Design and Magnet Material Grade at Different Temperatures and Gear Ratios. *IEEE Trans. Energy Convers.* **2021**, *36*, 2493–2501. [CrossRef]
62. Wong, H.Y.; Bird, J.Z.; Barnett, D.; Williams, W. A high torque density Halbach rotor coaxial magnetic gear. In Proceedings of the 2019 IEEE International Electric Machines & Drives Conference (IEMDC), San Deigo, CA, USA, 12–15 May 2019; IEEE: Piscataway, NJ, USA, 2019; pp. 233–239.
63. Praslicka, B.; Gardner, M.C.; Johnson, M.; Toliyat, H.A. Review and analysis of coaxial magnetic gear pole pair count selection effects. *IEEE J. Emerg. Sel. Top. Power Electron.* **2021**, *10*, 1813–1822. [CrossRef]
64. Atallah, K.; Howe, D. A novel high-performance magnetic gear. *IEEE Trans. Magn.* **2001**, *37*, 2844–2846. [CrossRef]
65. Dobzhanskyi, O.; Hossain, E.; Amiri, E.; Gouws, R.; Grebenikov, V.; Mazurenko, L.; Pryjmak, M.; Gamaliia, R. Axial-flux PM disk generator with magnetic gear for oceanic wave energy harvesting. *IEEE Access* **2019**, *7*, 44813–44822. [CrossRef]
66. Johnson, M.; Gardner, M.C.; Toliyat, H.A.; Englebretson, S.; Ouyang, W.; Tschida, C. Design, construction, and analysis of a large-scale inner stator radial flux magnetically geared generator for wave energy conversion. *IEEE Trans. Ind. Appl.* **2018**, *54*, 3305–3314. [CrossRef]
67. Atallah, K.; Wang, J.; Howe, D. A high-performance linear magnetic gear. *J. Appl. Phys.* **2005**, *97*, 10N516. [CrossRef]
68. Padinharu, D.K.K.; Li, G.J.; Zhu, Z.Q.; Clark, R.; Thomas, A.; Azar, Z.; Duke, A. Permanent Magnet Vernier Machines for Direct-Drive Offshore Wind Power: Benefits and Challenges. *IEEE Access* **2022**, *10*, 20652–20668. [CrossRef]
69. Kim, B.; Lipo, T.A. Operation and design principles of a PM vernier motor. In Proceedings of the 2013 IEEE Energy Conversion Congress and Exposition, Denver, CO, USA, 15–19 September 2013; IEEE: Piscataway, NJ, USA, 2013; pp. 5034–5041.
70. Zhou, Y.; Qu, R.; Shi, C.; Gao, Y. Analysis of thrust performance of a dual-mover linear vernier machine with horizontal-magnetized PM arrays. *IEEE Trans. Energy Convers.* **2018**, *33*, 2143–2152. [CrossRef]
71. Botha, C.D.; Kamper, M.J.; Wang, R.J.; Chama, A. Analytical modeling of surface-mounted and consequent-pole linear vernier hybrid machines. *IEEE Access* **2021**, *9*, 26251–26259. [CrossRef]
72. Liu, G.; Ding, L.; Zhao, W.; Chen, Q.; Jiang, S. Nonlinear equivalent magnetic network of a linear permanent magnet vernier machine with end effect consideration. *IEEE Trans. Magn.* **2017**, *54*, 1–9. [CrossRef]
73. Ghods, M.; Faiz, J.; Bazrafshan, M.; Arianborna, M. A Mesh Design Technique for Double Stator Linear PM Vernier Machine based on Equivalent Magnetic Network Modeling. *IEEE Trans. Energy Convers.* **2021**, *37*, 1087–1095. [CrossRef]
74. Zhao, W.; Ma, A.; Ji, J.; Chen, X.; Yao, T. Multiobjective optimization of a double-side linear Vernier PM motor using response surface method and differential evolution. *IEEE Trans. Ind. Electron.* **2019**, *67*, 80–90. [CrossRef]
75. Zhao, W.; Yao, T.; Xu, L.; Chen, X.; Song, X. Multi-objective optimization design of a modular linear permanent-magnet vernier machine by combined approximation models and differential evolution. *IEEE Trans. Ind. Electron.* **2020**, *68*, 4634–4645. [CrossRef]
76. Li, W.; Chau, K.; Liu, C.; Gao, S.; Wu, D. Analysis of tooth-tip flux leakage in surface-mounted permanent magnet linear vernier machines. *IEEE Trans. Magn.* **2013**, *49*, 3949–3952. [CrossRef]
77. Ivanova, I.A.; Agren, O.; Bernhoff, H.; Leijon, M. Simulation of wave-energy converter with octagonal linear generator. *IEEE J. Ocean. Eng.* **2005**, *30*, 619–629. [CrossRef]
78. Oprea, C.; Martis, C.; Jurca, F.; Fodorean, D.; Szabó, L. Permanent magnet linear generator for renewable energy applications: Tubular vs. four-sided structures. In Proceedings of the 2011 International Conference on Clean Electrical Power (ICCEP), Ischia, Italy, 14–16 June 2011; IEEE: Piscataway, NJ, USA, 2011; pp. 588–592.
79. Liu, Z.; Zhao, W.; Ji, J.; Chen, Q. A novel double-stator tubular vernier permanent-magnet motor with high thrust density and low cogging force. *IEEE Trans. Magn.* **2015**, *51*, 1–7.

80. Raihan, M.; Baker, N.; Smith, K.; Almoraya, A. An E-core linear veriner hybrid permanent magnet machine with segmented translator for direct drive wave energy converter. In Proceedings of the 2017 IEEE International Electric Machines and Drives Conference (IEMDC), Miami, FL, USA, 21–24 May 2017; IEEE: Piscataway, NJ, USA, 2017; pp. 1–6.
81. Baker, N.J.; Raihan, M.A.; Almoraya, A.A. A cylindrical linear permanent magnet Vernier hybrid machine for wave energy. *IEEE Trans. Energy Convers.* **2018**, *34*, 691–700. [CrossRef]
82. Baloch, N.; Khaliq, S.; Kwon, B.I. A high force density HTS tubular vernier machine. *IEEE Trans. Magn.* **2017**, *53*, 1–5.
83. Zhu, Z.Q.; Shuraiji, A.L.; Lu, Q.; Li, Y.; Qu, H. Novel Single-Phase Short-Stroke Tubular Permanent Magnet Oscillating Machines with Partitioned Stator. *Energies* **2021**, *14*, 1863. [CrossRef]
84. Sun, Y.; Xu, Z.; Zhang, Q.; Lu, J.; Liu, L. A Tubular Single-Phase Linear Generator with an Axially Magnetized PM Mover for Free-Piston Engines. *IEEJ Trans. Electr. Electron. Eng.* **2021**, *16*, 139–146. [CrossRef]
85. Zhao, M.; Zhang, Z.; Zhang, H.; Xu, Y.; Zou, J. Design and optimization of tubular linear vernier generator for direct drive wave energy converter. In Proceedings of the 2021 13th International Symposium on Linear Drives for Industry Applications (LDIA), Wuhan, China, 1–3 July 2021; IEEE: Piscataway, NJ, USA, 2021; pp. 1–6.
86. Mao, Y.X.; Liu, G.H.; Zhao, W.X.; Ji, J.H.; Zeng, Y.; Zheng, J.Q. Normal force and vibration investigation of linear permanent-magnet vernier machine. In Proceedings of the 2015 IEEE International Conference on Applied Superconductivity and Electromagnetic Devices (ASEMD), Shanghai, China, 20–23 November 2015; IEEE: Piscataway, NJ, USA, 2015; pp. 137–138.
87. Kosuge, Y.; Kataoka, Y.; Takayama, M.; Matsusima, Y.; Anazawa, Y. Development of surface permanent magnet-type linear vernier motor. In Proceedings of the 2015 18th International Conference on Electrical Machines and Systems (ICEMS), Pattaya , Thailand, 25–28 October 2015; IEEE: Piscataway, NJ, USA, 2015; pp. 248–253.
88. Wang, S.; Zhao, W.; Kang, M. Design and analysis of double-sided linear primary permanent magnet vernier motor. In Proceedings of the 2016 19th International Conference on Electrical Machines and Systems (ICEMS), Chiba, Japan, 13–16 November 2016; IEEE: Piscataway, NJ, USA, 2016; pp. 1–5.
89. Zhu, X.; Ji, J.; Xu, L.; Kang, M. Design and analysis of dual-stator PM vernier linear machine with PMs surface-mounted on the mover. *IEEE Trans. Appl. Supercond.* **2017**, *28*, 1–5. [CrossRef]
90. Li, W.; Ching, T. A new segmented-stator linear vernier permanent magnet machine for direct-drive applications. In Proceedings of the 2017 IEEE International Electric Machines and Drives Conference (IEMDC), Miami, FL, USA, 21–24 May 2017; IEEE: Piscataway, NJ, USA, 2017; pp. 1–6.
91. Li, D.; Qu, R.; Li, J.; Xu, W. Consequent-pole toroidal-winding outer-rotor Vernier permanent-magnet machines. *IEEE Trans. Ind. Appl.* **2015**, *51*, 4470–4481. [CrossRef]
92. Almoraya, A.; Baker, N.; Smith, K.; Raihan, M. Development of a double-sided consequent pole linear vernier hybrid permanent-magnet machine for wave energy converters. In Proceedings of the 2017 IEEE International Electric Machines and Drives Conference (IEMDC), Miami, FL, USA, 21–24 May 2017; IEEE: Piscataway, NJ, USA, 2017; pp. 1–7.
93. Liu, X.; Zou, C.; Du, Y.; Xiao, F. A linear consequent pole stator permanent magnet vernier machine. In Proceedings of the 2014 17th International Conference on Electrical Machines and Systems (ICEMS), Hangzhou, China, 22–25 October 2014; IEEE: Piscataway, NJ, USA, 2014; pp. 1753–1756.
94. Shi, C.; Qu, R.; Gao, Y.; Li, D.; Jing, L.; Zhou, Y. Design and analysis of an interior permanent magnet linear vernier machine. *IEEE Trans. Magn.* **2018**, *54*, 1–5.
95. Xu, X.; Fan, Z.; Ai, L.; Feng, H.; Du, B.; Zhao, Y. Characteristic analysis and optimization of U-PM linear vernier motor. In Proceedings of the 2021 13th International Symposium on Linear Drives for Industry Applications (LDIA), Wuhan, China, 1–3 July 2021; IEEE: Piscataway, NJ, USA, 2021; pp. 1–5.
96. Du, K.; Zhao, W.; Xu, L.; Ji, J. Design of a new fault-tolerant linear permanent-magnet vernier machine. *IEEE J. Emerg. Sel. Top. Ind. Electron.* **2020**, *1*, 172–181. [CrossRef]
97. Vining, J.; Mundon, T.; Nair, B. Electromechanical design and experimental evaluation of a double-sided, dual airgap linear vernier generator for wave energy conversion. In Proceedings of the 2017 IEEE Energy Conversion Congress and Exposition (ECCE), Cincinnati, OH, USA, 1–5 October 2017; IEEE: Piscataway, NJ, USA, 2017; pp. 5557–5564.
98. Seifert, R.; Micklitz, T.; Mößner, B.; Hofmann, W. Methodologies for the analytical design of tubular linear vernier synchronous generators with quasi-halbach-magnetization. In Proceedings of the 2018 XIII International Conference on Electrical Machines (ICEM), Alexandroupoli, Greece, 3–6 September 2018; IEEE: Piscataway, NJ, USA, 2018; pp. 2235–2242.
99. Huo, Y.; Qu, R.; Gao, Y.; Jia, S.; Fan, X. Design of a linear vernier permanent magnet machine with high thrust force density and low thrust force ripple. In Proceedings of the 2017 IEEE International Electric Machines and Drives Conference (IEMDC), Miami, FL, USA, 21–24 May 2017; IEEE: Piscataway, NJ, USA, 2017; pp. 1–6.
100. Choi, G. Analysis and Experimental Verification of the Demagnetization Vulnerability in Various PM Synchronous Machine Configurations for an EV Application. *Energies* **2021**, *14*, 5447. [CrossRef]
101. Almoraya, A.A.; Baker, N.; Smith, K.; Raihan, M. A new configuration of a consequent pole linear vernier hybrid machine with V-shape magnets. In Proceedings of the 2018 XIII International Conference on Electrical Machines (ICEM), Alexandroupoli, Greece, 3–6 September 2018; IEEE: Piscataway, NJ, USA, 2018; pp. 2002–2008.
102. Shi, C.; Qu, R.; Li, D.; Ren, X.; Gao, Y.; Chen, Z. Analysis of the fractional pole-pair linear PM vernier machine for force ripple reduction. *IEEE Trans. Ind. Electron.* **2020**, *68*, 4748–4759. [CrossRef]

103. Zhang, H.; Shao, Y.; Kou, B.; Qu, R.; Zhu, Z. Comparative study of double-sided toroidal-winding linear PM vernier machines with different secondary configurations. In Proceedings of the 2017 20th International Conference on Electrical Machines and Systems (ICEMS), Sydney, Australia, 11–14 August 2017; IEEE: Piscataway, NJ, USA, 2017; pp. 1–5.
104. Zhang, H.; Kou, B.; Shao, Y.; Qu, R. Comparison of toroidal-winding linear PM vernier machines with typical linear synchronous machines in aspect of thrust force characteristics. In Proceedings of the 2019 12th International Symposium on Linear Drives for Industry Applications (LDIA), Neuchatel, Switzerland, 1–3 July 2019; IEEE: Piscataway, NJ, USA, 2019; pp. 1–5.
105. Ma, A.; Zhao, W.; Xu, L.; Ji, J.; Bian, F. Influence of armature windings pole numbers on performances of linear permanent-magnet vernier machines. *IEEE Trans. Transp. Electrif.* **2019**, *5*, 385–394. [CrossRef]
106. Ji, J.; Zhao, W.; Fang, Z.; Zhao, J.; Zhu, J. A novel linear permanent-magnet vernier machine with improved force performance. *IEEE Trans. Magn.* **2015**, *51*, 1–10. [CrossRef]
107. Zhao, W.; Zheng, J.; Wang, J.; Liu, G.; Zhao, J.; Fang, Z. Design and analysis of a linear permanent-magnet vernier machine with improved force density. *IEEE Trans. Ind. Electron.* **2015**, *63*, 2072–2082. [CrossRef]
108. Shi, C.; Li, D.; Qu, R.; Zhang, H.; Gao, Y.; Huo, Y. A novel linear permanent magnet Vernier machine with consequent-pole permanent magnets and Halbach permanent magnet arrays. *IEEE Trans. Magn.* **2017**, *53*, 1–4. [CrossRef]
109. Wu, F.; El-Refaie, A.M. Permanent magnet vernier machine: A review. *IET Electr. Power Appl.* **2019**, *13*, 127–137. [CrossRef]
110. Liu, Y.; Li, H.; Zhu, Z. A high-power factor vernier machine with coil pitch of two slot pitches. *IEEE Trans. Magn.* **2018**, *54*, 1–5.
111. Wang, S.Y.; Zhao, W.X.; Ji, J.H.; Zheng, J.Q. Pole ratio effect on performances of linear permanent magnet vernier motor. In Proceedings of the 2015 IEEE International Conference on Applied Superconductivity and Electromagnetic Devices (ASEMD), Shanghai, China, 20–23 November 2015; IEEE: Piscataway, NJ, USA, 2015; pp. 183–184.
112. Zhao, W.; Du, K.; Xu, L. Design considerations of fault-tolerant permanent magnet vernier machine. *IEEE Trans. Ind. Electron.* **2019**, *67*, 7290–7300. [CrossRef]
113. Wang, S.; Zhao, W.; Ji, J.; Xu, L.; Zheng, J. Magnetic gear ratio effects on performances of linear primary permanent magnet vernier motor. *IEEE Trans. Appl. Supercond.* **2016**, *26*, 1–5. [CrossRef]
114. Khaliq, S.; Kwon, B.i. Design and analysis of a dual-stator spoke-type linear vernier machine for wave energy extraction. *J. Electr. Eng. Technol.* **2016**, *11*, 1700–1706. [CrossRef]
115. Arish, N. Electromagnetic performance analysis of linear vernier machine with PM and HTS-Bulk. *Phys. C Supercond. Appl.* **2020**, *579*, 1353751. [CrossRef]
116. Liu, B.; Badcock, R.; Shu, H.; Tan, L.; Fang, J. Electromagnetic characteristic analysis and optimization design of a novel HTS coreless induction motor for high-speed operation. *IEEE Trans. Appl. Supercond.* **2018**, *28*, 1–5. [CrossRef]
117. Li, W.; Ching, T.; Chau, K. Design and analysis of a new parallel-hybrid-excited linear vernier machine for oceanic wave power generation. *Appl. Energy* **2017**, *208*, 878–888. [CrossRef]
118. Ching, T.; Li, W.; Chau, K. A new parallel-hybrid-excitation linear vernier permanent-magnet machine: Improved solution for direct-driven power generation. In Proceedings of the 2016 Eleventh International Conference on Ecological Vehicles and Renewable Energies (EVER), Monte Carlo, Monaco, 6–8 April 2016; IEEE: Piscataway, NJ, USA, 2016; pp. 1–5.
119. Baloch, N.; Khaliq, S.; Kwon, B.I. HTS dual-stator spoke-type linear vernier machine for leakage flux reduction. *IEEE Trans. Magn.* **2017**, *53*, 1–4.
120. Ching, T.; Chau, K.; Li, W. Power factor improvement of a linear vernier permanent-magnet machine using auxiliary DC field excitation. *IEEE Trans. Magn.* **2016**, *52*, 1–4. [CrossRef]
121. Li, W.; Ching, T.; Chau, K. A new linear vernier permanent-magnet machine using high-temperature superconducting DC field excitation. *IEEE Trans. Appl. Supercond.* **2017**, *27*, 1–5. [CrossRef]
122. Zhou, Y.; Gao, Y.; Qu, R.; Cheng, Y.; Shi, C. A novel dual-stator HTS linear vernier generator for direct drive marine wave energy conversion. *IEEE Trans. Appl. Supercond.* **2019**, *29*, 1–6. [CrossRef]
123. Du, Y.; Chau, K.; Cheng, M.; Fan, Y.; Zhao, W.; Li, F. A linear stator permanent magnet vernier HTS machine for wave energy conversion. *IEEE Trans. Appl. Supercond.* **2012**, *22*, 5202505. [CrossRef]
124. Zhang, H.; Kou, B.; Zhu, Z.Q.; Qu, R.; Luo, J.; Shao, Y. Thrust ripple analysis on toroidal-winding linear permanent magnet vernier machine. *IEEE Trans. Ind. Electron.* **2018**, *65*, 9853–9862. [CrossRef]
125. Hu, H.; Zhao, J.; Liu, X.; Guo, Y. Magnetic field and force calculation in linear permanent-magnet synchronous machines accounting for longitudinal end effect. *IEEE Trans. Ind. Electron.* **2016**, *63*, 7632–7643. [CrossRef]
126. Hu, H.; Liu, X.; Zhao, J.; Guo, Y. Analysis and minimization of detent end force in linear permanent magnet synchronous machines. *IEEE Trans. Ind. Electron.* **2017**, *65*, 2475–2486. [CrossRef]
127. Bianchi, N.; Bolognani, S.; Cappello, A. Reduction of cogging force in PM linear motors by pole-shifting. *IEE Proc. Electr. Power Appl.* **2005**, *152*, 703–709. [CrossRef]
128. Baker, N.J.; Raihan, M.A.; Almoraya, A.A.; Burchell, J.W.; Mueller, M.A. Evaluating alternative linear vernier hybrid machine topologies for integration into wave energy converters. *IEEE Trans. Energy Convers.* **2018**, *33*, 2007–2017. [CrossRef]
129. Zhou, Y.; Shi, C.; Qu, R.; Li, D.; Gao, Y.; Li, R. A novel consequent-pole modular-mover linear permanent magnet vernier machine for thrust ripple and cost reduction. *IEEE Trans. Ind. Appl.* **2021**, *57*, 5841–5850. [CrossRef]
130. Du, Y.; Cheng, M.; Chau, K.T.; Liu, X.; Xiao, F.; Zhao, W. Linear primary permanent magnet vernier machine for wave energy conversion. *IET Electr. Power Appl.* **2015**, *9*, 203–212. [CrossRef]

131. Naderi, P.; Sharouni, S.; Moradzadeh, M. Linear vernier machine wave converter modelling and analysis by MEC. *IET Electr. Power Appl.* **2020**, *14*, 751–761. [CrossRef]
132. Nematsaberi, A.; Faiz, J. A novel linear stator-PM Vernier machine with spoke-type magnets. *IEEE Trans. Magn.* **2018**, *54*, 1–5. [CrossRef]
133. Almoraya, A.A.; Baker, N.J.; Smith, K.J.; Raihan, M.A. Design and analysis of a flux-concentrated linear vernier hybrid machine with consequent poles. *IEEE Trans. Ind. Appl.* **2019**, *55*, 4595–4604. [CrossRef]
134. Eguren, I.; Almandoz, G.; Egea, A.; Elorza, L.; Urdangarin, A. Development of a thermal analysis tool for linear machines. *Appl. Sci.* **2021**, *11*, 5818. [CrossRef]
135. Huang, Z.; Fang, J.; Liu, X.; Han, B. Loss calculation and thermal analysis of rotors supported by active magnetic bearings for high-speed permanent-magnet electrical machines. *IEEE Trans. Ind. Electron.* **2015**, *63*, 2027–2035. [CrossRef]
136. Tekgun, B.; Sozer, Y.; Tsukerman, I.; Upadhyay, P.; Englebretson, S. Core loss estimation in electric machines with flux-controlled core loss tester. *IEEE Trans. Ind. Appl.* **2018**, *55*, 1299–1308. [CrossRef]
137. Curti, M.; Van Beek, T.; Jansen, J.; Gysen, B.; Lomonova, E. General formulation of the magnetostatic field and temperature distribution in electrical machines using spectral element analysis. *IEEE Trans. Magn.* **2018**, *54*, 1–9. [CrossRef]